Journal of Sound and Vibration 329 (2010) 2768–2791

Contents lists available at ScienceDirect

Journal of Sound and Vibration

journal homepage: www.elsevier.com/locate/jsvi

Experimental study of targeted energy transfer from an acoustic system to a nonlinear membrane absorber

R. Bellet, B. Cochelin *, P. Herzog, P.-O. Mattei

Laboratoire de Mécanique et d'Acoustique, UPR CNRS 7051, 31 chemin Joseph-Aiguier, 13402 Marseille Cedex 20, France

ARTICLE INFO

Article history:
Received 21 December 2009
Received in revised form
26 January 2010
Accepted 26 January 2010
Handling Editor: L.G. Tham
Available online 18 February 2010

ABSTRACT

This paper deals with the application of the concept of targeted energy transfer to the field of acoustics, providing a new approach to passive sound control in the low frequency domain, where no efficient dissipative mechanism exists. The targeted energy transfer, also called energy pumping, is a phenomenon that we observe by combining a pure nonlinear oscillator with a linear primary system. It corresponds to an almost irreversible transfer of vibration energy from the linear system to the auxiliary nonlinear one, where the energy is finally dissipated. In this study, an experimental set-up has been developed using the air inside a tube as the acoustic linear system, a thin circular visco-elastic membrane as an essentially cubic oscillator and the air inside a box as a weak coupling between those two elements. In this paper, which mainly deals with experimental results, it is shown that several regimes exist under sinusoidal forcing, corresponding to the different nonlinear normal modes of the system. One of these regimes is the quasi-periodic energy pumping regime. The targeted energy transfer phenomenon is also visible on the free oscillations of the system. Indeed, above an initial excitation threshold, the sound extinction in the tube follows a quasi-linear decrease that is much faster than the usual exponential one. During this linear decrease, the energy of the acoustic medium is irreversibly transferred to the membrane and then damped into this element called nonlinear energy sink. We present also the frequency responses of the system which shows a clipping of the original resonance peak of the acoustic medium and we finally demonstrate the ability of the nonlinear absorber to operate in a large frequency band, tuning itself to any linear system.

1. Introduction

To reduce the level of noise and vibration that arises in many engineering applications, specific devices called ''dynamic absorbers'' or ''absorbers'' are often used. In Acoustics, classical absorbers are porous materials for high frequencies and Helmholtz resonators for low frequencies. In mechanics, the most popular device is the tuned mass-damper system known as the Frahm absorber. Most of these absorbers are linear devices [1–6] that rely on the anti-resonance concept. It has been recently established that the use of a pure nonlinear absorber, consisting of a mass with an essentially nonlinear spring, can provide a useful alternative solution to reduce vibrations. The dynamics of such a nonlinear absorber associated to a linear primary system, which differs radically from those of classical linear absorbers, have been described in detail in

* Corresponding author. Tel.: +33 4 91 16 40 07; fax: +33 4 91 71 28 66.
E-mail addresses: bellet@lma.cnrs-mrs.fr (R. Bellet), bruno.cochelin@ec-marseille.fr (B. Cochelin), herzog@lma.cnrs-mrs.fr (P. Herzog), mattei@lma.cnrs-mrs.fr (P.-O. Mattei).

0022-460X/$ - see front matter © 2010 Elsevier Ltd. All rights reserved.
doi:10.1016/j.jsv.2010.01.029

[7–11] in terms of resonance capture and nonlinear normal modes. The first experimental demonstration of these behaviours was described in [12]. The principle consists in placing the absorber in a situation where an irreversible transfer of vibration energy occurs from the linear system to the absorber. This energy is finally damped in the absorber. The result is an efficient cancellation of the vibrations in the linear system, since the motion gets localized in the absorber. This phenomenon is called targeted energy transfer or energy pumping in the literature.

One interesting feature of these nonlinear absorbers is the fact that they operate in a given large frequency band, instead of "close to a single frequency", as in the case of classical Frahm absorbers or Helmholtz resonators. Indeed, it is worth noting that, since the spring of the absorber is essentially nonlinear, this system has no natural frequency. One of the drawbacks of nonlinear absorbers is the fact that the irreversible energy transfer occurs only when the primary linear system reaches a certain vibration energy threshold. This can be a limitation in the case of some practical applications. Systems in which a nonlinear oscillator is coupled to various kind of linear primary systems have been previously studied: a wave guide [13], a rod [14–16], a beam [17], a plate [18], a two degrees of freedom (dof) linear system [19] or a linear chain of coupled oscillators [20]. In the field of engineering, the application of targeted energy transfer phenomena has been explored to control aeroelastic instabilities [21,22], for seismic mitigation in civil engineering [23,24] and to stabilize drill-string systems [25]. Moreover some investigations have been done about the kind of nonlinearity: vibro-impact absorber [26], non-polynomial nonlinearity [27], multidegree of freedom nonlinear absorber [28–31]. Further details about the theory and the advantages and drawbacks of such nonlinear absorbers can be found in a recent book by Vakakis et al. [32].

In the present study, the primary linear system is an acoustic medium and the nonlinear absorber is a thin visco-elastic membrane which is connected to the acoustic medium and is subjected to very large oscillations, i.e. very larger than the thickness of the membrane. Using an improved version of the experimental set-up presented in [33], we investigated the targeted energy transfer occurring between the acoustic medium and the membrane during both the sinusoidal forced regime and the free oscillations. The experimental data were analysed using various tools and methods (wavelet transform, frequency–energy plot, energy exchange diagram) so as to demonstrate and characterize the transfer. A simple two dof model has also been developed and the predictions of this model have been compared with the experimental data. Moreover the different frequency responses of the system have been experimentally measured and numerically simulated. Finally, by changing the primary acoustic system, the last part of the present study demonstrates the ability of the membrane to operate in a large frequency band tuning itself to several different resonance frequencies. All these results pave the way to design new kinds of passive vibro-acoustical absorbers in the low frequency domain where no efficient dissipative mechanism exists.

2. The system under investigation

2.1. The classical two degrees of freedom mechanical system

To analyse the targeted energy transfer, many authors have used simple mechanical systems with two degrees of freedom. A mass and a linear spring stand for the linear system to be protected, and a mass associated with an essentially nonlinear spring and a damper stands for the dynamic absorber. A weak coupling spring is placed between the two oscillators as shown in Fig. 1. Because the nonlinear oscillator is connected to the ground, this configuration is referred to as the "grounded configuration". Targeted energy transfer typically occurs when the mass of the nonlinear system is of the same order as the mass of the linear oscillator and when the stiffness of the coupling between the two oscillators is small.

Let $u_1(t)$ and $u_2(t)$ be the displacement of the masses, and assuming a cubic restoring force by the nonlinear spring, the governing equations (nondimensional form) of the grounded configuration are

$$\ddot{u}_1 + a\dot{u}_1 + u_1 + b(u_1 - u_2) = 0,$$

$$c\ddot{u}_2 + d\dot{u}_2 + eu_2^3 + b(u_2 - u_1) = 0, \tag{1}$$

where b is a small coupling coefficient, c is the mass ratio, a and d are, respectively, the damping factors in the linear and nonlinear oscillators and e is the cubic stiffness coefficient.

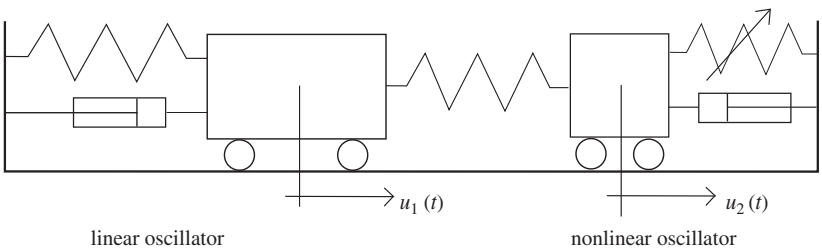

Fig. 1. The grounded two dof mechanical system classically used to study the energy pumping phenomenon.

Despite its simplicity, a system of this kind has highly complex dynamics which have been thoroughly studied in [34–43]. Without going into detail, we recall that its dynamics can be enlighted by analysing the two nonlinear vibrating modes of the undamped system and the transition between these two modes. It should be added that some of these references deals with non-grounded configurations, where a small mass is directly connected to the linear mass via a cubic spring. This is not of great importance, since the behaviour of the grounded and non-grounded configuration is very similar.

2.2. The vibro-acoustical experimental set-up

2.2.1. Principle

The simple two dof spring-mass system described above served here as a basis for designing an experimental set-up (Fig. 2) in which the primary system is an acoustic medium.

As the linear primary system, we consider the first acoustic mode of an open/open tube having length L and section S_t. When the air inside the tube vibrates on this mode, the acoustic pressure is almost zero at the ends of the tube and maximum at the centre, whereas the velocity of the air is maximum at the ends and zero at the center. A discrete simplified representation of this vibrating mode can be obtained by considering two concentrated masses of air that move with the same amplitude but in opposite directions at the ends of the tube, and are connected by a spring representing the compressibility of the air. This constitutes an analogy of a one degree of freedom mechanical spring-mass system. The aim is then to act on that system, thanks to a nonlinear absorber, in order to reduce its vibrations. Today, the design of a purely acoustic system that would reproduce an analogy to a mechanical nonlinear absorber is still an open question. In this study, the nonlinear absorber is a mechanical one: it is a simple thin circular visco-elastic membrane that performs very large amplitude oscillations in order to obtain an almost purely cubic response. The coupling between the tube and the membrane is ensured acoustically by the air in a coupling box, which is sufficiently large to give a weak linear coupling stiffness.

2.2.2. The set-up realization

The experimental set-up based on these principles has been realized and made it possible to observe the targeted energy transfer (energy pumping) phenomenon from the acoustic medium to the visco-elastic membrane (Fig. 3).

In practical terms, the tube (the linear system) is an interchangeable U-shaped tube so that its length L can be adjusted between 1.5 and 2.5 m. The first resonance frequency corresponding to these lengths therefore ranges between around 75 and 120 Hz. Since the diameter of the tube d=94 mm is small in comparison to L, the tube could be either straight or U-shaped. The volume of the coupling box is $V_2=27\times10^{-3}\,\mathrm{m}^3$. The device which holds the membrane allows to change the diameter of the working part from 40 to 80 mm. A sliding system is used to apply a constant in-plane pre-stress to the membrane. Once the pre-stress is set, the membrane is clamped to the supporting device. The material used is latex and silicone, with a Young's modulus of about 1.4 MPa, a Poisson's ratio of about 0.49 and a volume mass density of about $1000\,\mathrm{kg\,m^{-3}}$. Various thicknesses h ranging between 0.18 and 1 mm have been tested.

For the excitation of the tube, we use an acoustic source consisting of a loudspeaker and a coupling box which is connected to the entrance of the tube. An analyser controls the excitation and collects two measurements: the acoustic pressure at the center of the tube (microphone) and the velocity of the center of the membrane (laser vibrometer). It should be noticed that this set-up is an improved version of the one presented in a previous paper [33]. Thanks to this improvement, we have now more possibilities to vary the different physical parameters, a better control of them and a better clamped limit condition for the membrane (see Fig. 3).

2.3. Associated models

In this section, we present a simple model for the experimental set-up described above. The acoustic medium and the nonlinear absorber are both modelled as single dof spring-mass systems, leading to a two dof system.

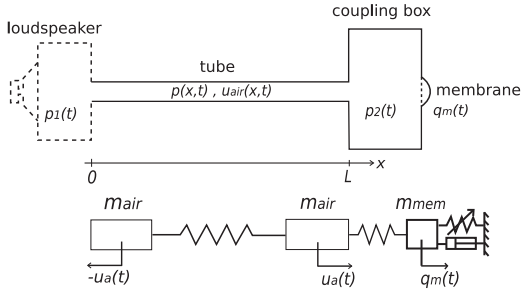

Fig. 2. Scheme and principle of the set-up.

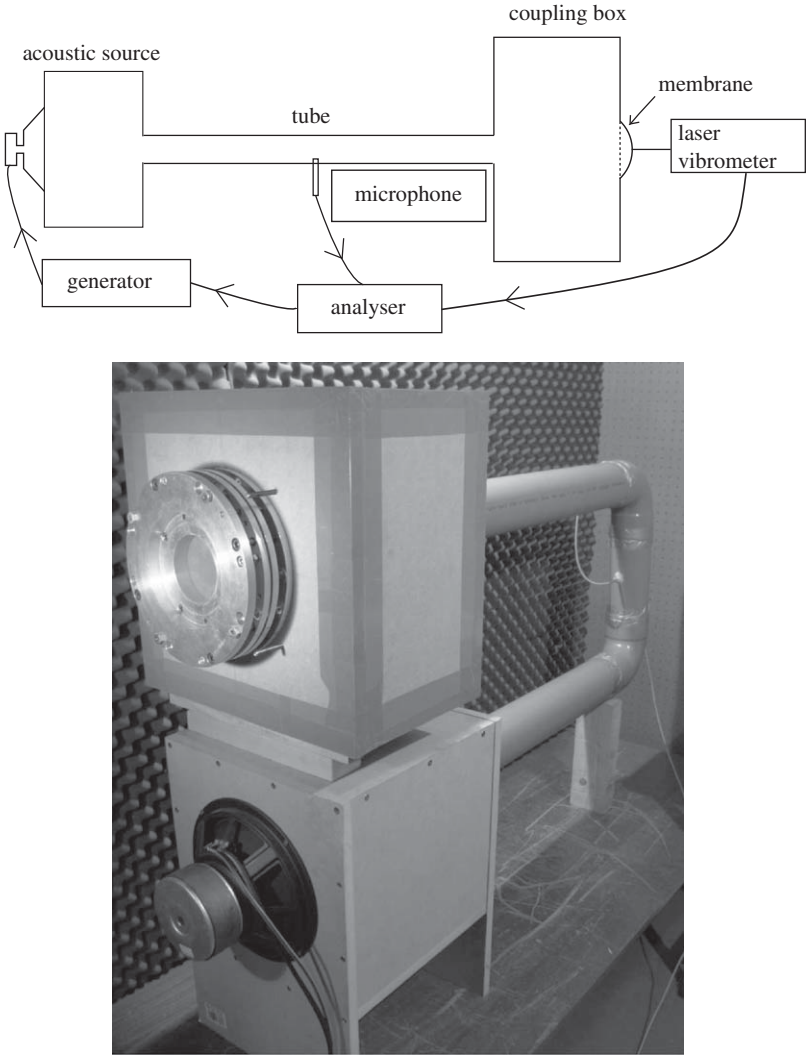

Fig. 3. Scheme and picture of the set-up.

2.3.1. The tube

Because the length of the tube is large in comparison with its diameter, the system is assumed to be one-dimensional. Let $u_{\text{air}}(x,t)$ and $p(x,t)$ be the acoustic displacement and the pressure, respectively. The motion of the air in the tube is governed by the following conservation equation and constitutive law:

$$\rho_a \frac{\partial^2 u_{\text{air}}}{\partial t^2} = -\frac{\partial p}{\partial x} \quad \text{and} \quad p = -\rho_a c_0^2 \frac{\partial u_{\text{air}}}{\partial x}, \tag{2}$$

with the boundary conditions $p(0,t)=p_1(t)$ and $p(L,t)=p_2(t)$. Here, ρ_a is the density of the air and c_0 is the sound wave velocity. To apply a one dof Rayleigh–Ritz reduction, we write these equations in the following variational form:

$$\int_0^L \rho_a S_t \frac{\partial^2 u_{\text{air}}}{\partial t^2} \delta u_{\text{air}} \, \mathrm{d}x = -\int_0^L \rho_a S_t c_0^2 \frac{\partial u_{\text{air}}}{\partial x} \frac{\partial \delta u_{\text{air}}}{\partial x} \, \mathrm{d}x - p_2(t) S_t \delta u_{\text{air}}(L,t) + p_1(t) S_t \delta u_{\text{air}}(0,t), \tag{3}$$

and we take a shape function for $u_{\text{air}}(x,t)$ which is exactly the first acoustic mode of the tube. We denote by u_a the displacement of the air at the end of the tube ($x=L$). It is positive when the air goes out:

$$u_{\text{air}}(x,t) = u_a(t)\left(-\cos\left(\frac{\pi x}{L}\right)\right), \quad \delta u_{\text{air}}(x,t) = \delta u_a(t)\left(-\cos\left(\frac{\pi x}{L}\right)\right). \tag{4}$$

The Rayleigh–Ritz reduction yields the following differential equation:

$$\left(\frac{\rho_a S_t L}{2}\right)\ddot{u}_a + \left(\frac{\rho_a S_t c_0^2 \pi^2}{2L}\right) u_a = -p_1 S_t - p_2 S_t. \tag{5}$$

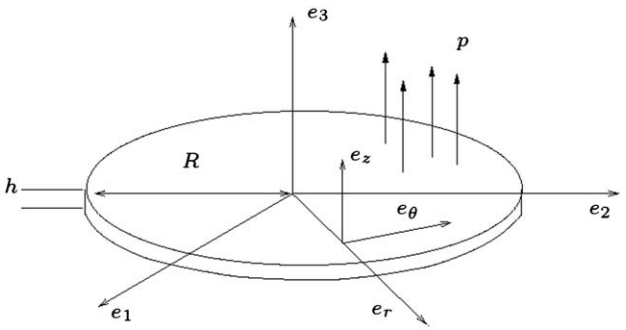

Fig. 4. Scheme of the membrane.

We now account for the damping of the mode by introducing a viscous term with a coefficient c_f. Finally, we get

$$m_a\ddot{u}_a + c_f\dot{u}_a + k_a u_a = -p_1 S_t - p_2 S_t, \tag{6}$$

where

$$m_a = \frac{\rho_a S_t L}{2}, \quad k_a = \frac{\rho_a S_t c_0^2 \pi^2}{2L}. \tag{7}$$

2.3.2. The membrane

Under the pressure applied by the air in the coupling box, the thin visco-elastic circular clamped membrane performs large amplitude oscillations. Typically, the displacement at the center can be about 10 mm, which is 10–30 times larger than the membrane thickness. For the modeling (see Fig 4), we consider the nonlinear plate equation of the Von-Karman type (large displacements, small strains and moderate rotations) taking account of a constant in-plane pre-stress. Since the problem is axisymmetric, the displacement field is written as

$$\mathbf{u}(r,\theta,z) = \left(u(r) - \frac{\partial w(r)}{\partial r}\right)\mathbf{e}_r + w(r)\mathbf{e}_z. \tag{8}$$

The corresponding strain field tensor is $\mathbf{E} = \mathbf{e} + z\mathbf{k}$, where the components of the generalized tension and bending strain tensor $\mathbf{e}$ and $\mathbf{k}$ read

$$e_{rr} = \frac{\partial u}{\partial r} + \frac{1}{2}\left(\frac{\partial w}{\partial r}\right)^2, \quad e_{\theta\theta} = \frac{u}{r}, \quad e_{r\theta} = 0,$$

$$k_{rr} = -\frac{\partial^2 w}{\partial r^2}, \quad k_{\theta\theta} = -\frac{1}{r}\frac{\partial w}{\partial r}, \quad k_{r\theta} = 0. \tag{9}$$

The material of which the membrane is composed is assumed to obey a simple Kelvin–Voigt constitutive law. The stress tensor $\mathbf{S}$, the strain tensor $\mathbf{E}$ and the velocity strain tensor $\dot{\mathbf{E}}$ are related as follows:

$$\mathbf{S} = \mathbf{D} : (\mathbf{E} + \eta\dot{\mathbf{E}}), \tag{10}$$

where η is the viscous parameter and $\mathbf{D}$ is the fourth-order isotropic elastic tensor depending on Young's modulus E and Poisson's ratio v.

The generalized stress tensor (tension and bending) is accordingly

$$N_{rr} = \frac{Eh}{1-v^2}\left(e_{rr} + ve_{\theta\theta} + \eta(\dot{e_{rr}} + v\dot{e_{\theta\theta}})\right),$$

$$N_{\theta\theta} = \frac{Eh}{1-v^2}\left(e_{\theta\theta} + ve_{rr} + \eta(\dot{e_{\theta\theta}} + v\dot{e_{rr}})\right),$$

$$N_{r\theta} = 0,$$

$$M_{rr} = \frac{Eh^3}{12(1-v^2)}\left(k_{rr} + vk_{\theta\theta} + \eta\left(\dot{k_{rr}} + v\dot{k_{\theta\theta}}\right)\right),$$

$$M_{\theta\theta} = \frac{Eh^3}{12(1-v^2)}\left(k_{\theta\theta} + vk_{rr} + \eta\left(\dot{k_{\theta\theta}} + v\dot{k_{rr}}\right)\right),$$

$$M_{r\theta} = 0. \tag{11}$$

The displacement u^0, the strain e^0 and the stress N^0 associated with the constant pre-strain e_0 applied to the membrane are

$$u^0(r)=e_0 r, \quad e^0_{rr}=e^0_{\theta\theta}=e_0, \quad N^0_{rr}=N^0_{\theta\theta}=\frac{Eh}{1-\nu}e_0. \tag{12}$$

We now write the governing equation of the membrane using the virtual work principle:

$$-\int_{S_m}((N^0+N)\delta e+M\delta k)\,\mathrm{d}S+\int_{S_m}p_2\delta w\,\mathrm{d}S=\int_{S_m}\rho_m h\ddot{w}\delta w\,\mathrm{d}S. \tag{13}$$

Once again, we apply a Rayleigh–Ritz reduction with a single parabolic shape function to describe the transversal displacement of the membrane. The degree of freedom $q_m(t)$ is the transversal displacement of the center of the membrane.

$$w(r,t)=\left(\frac{R^2-r^2}{R^2}\right)q_m(t), \quad u(r,t)=0,$$

$$\delta w(r,t)=\frac{R^2-r^2}{R^2}\delta q(t), \quad \delta u(r,t)=0. \tag{14}$$

This gives the following one dof differential equation for $q_m(t)$:

$$m_m\ddot{q_m}+k_1[(1+\chi)q_m+\eta\dot{q_m}]+k_3(2\eta q_m^2\dot{q_m}+q_m^3)=\frac{S_m}{2}p_2(t), \tag{15}$$

where

$$m_m=\frac{\rho_m h S_m}{3}, \quad k_1=\frac{2\pi Eh^3}{3(1-\nu)R^2},$$

$$k_3=\frac{8\pi Eh}{3(1-\nu^2)R^2}, \quad \chi=\frac{3R^2e_0}{h^2}. \tag{16}$$

The coefficients k_1 and k_3, respectively, stand for the linear and nonlinear stiffnesses. The parameter χ is the ratio between the pre-strain e_0 and the (strain) buckling load of the membrane. The exact strain buckling load of a circular clamped plate is $14.68h^2/12(1+\nu)R^2$. Here, we get an approximate value $h^2/3R^2$ because of the parabolic shape function. The linear stiffness is zero when $\chi=-1$ (buckling) and it increases with positive values of χ. The term $1+\chi$ can be also be rewritten in the form $(f_1/f_0)^2$, where f_1 is the first resonance frequency of the membrane with pre-stress and f_0 the resonance frequency of the membrane without pre-stress: $f_0=(1/2\pi)\sqrt{1.015^4\pi^4Eh^2/12(1-\nu^2)\rho_a R^4}$ (as demonstrated in the book [44, table 2.1]). Since f_1 can be measured experimentally and we have an analytical expression for f_0, we prefer to use the ratio f_1/f_0 in the following.

It should be noted that the parabolic shape function shows a good fit with the description of the large amplitude oscillations, but not with the small amplitude ones or the buckling deflection. For instance, the zero slope condition is not even satisfied at the clamped boundary. In order to improve the linear part of this one dof model, we take the following modified expression of k_1:

$$k_1=\frac{1.015^4\pi^5}{36}\frac{Eh^3}{(1-\nu^2)R^2}, \tag{17}$$

so that k_1/m_m now corresponds to the first eigenvalue $(2\pi f_0)^2$ of the circular clamped plate.

2.3.3. The coupling box

The volume of the coupling box is chosen large enough to behave like a weak coupling, but its dimensions remain small enough, in comparison to the considered range of wavelength (around 4 m), to assume that the pressure p_2 inside the box is spatially constant. This pressure is related to the relative variation of the volume $\Delta V_2/V_2$ due to the motion of the membrane and of the air inside the tube as follows:

$$p_2(t)=\rho_a c_0^2\frac{\Delta V_2}{V_2}=k_b\left[S_t u_a(t)-\frac{S_m}{2}q_m(t)\right] \quad \text{with } k_b=\frac{\rho_a c_0^2}{V_2}. \tag{18}$$

2.3.4. The excitation

For the sake of simplicity, we do not model the box at the entrance of the tube, the loudspeaker and the system that supply the loudspeaker. We assume that this excitation system provides a periodic pressure:

$$p_1(t)=P_1\cos(\Omega t) \tag{19}$$

that acts as a source at the entrance of the tube with an amplitude P_1 and a frequency Ω.

2.3.5. The final dimensional and non-dimensional two dof system

Inserting expressions (18) and (19) into Eqs. (6) and (15), we obtain the following final two dof system:

$$m_a\ddot{u}_a+c_f\dot{u}_a+k_au_a+S_tk_b\left(S_tu_a-\frac{S_m}{2}q_m\right)=F\cos(\Omega t),$$

$$m_m\ddot{q}_m+k_1\left[\left(\frac{f_1}{f_0}\right)^2q_m+\eta\dot{q}_m\right]+k_3[q_m^3+2\eta q_m^2\dot{q}_m]+\frac{S_m}{2}k_b\left(\frac{S_m}{2}q_m-S_tu_a\right)=0. \tag{20}$$

Nondimensional quantities are introduced by normalizing q_m with the membrane thickness h and u_a with h and a section ratio for u_a. The time is normalized with the first frequency of the tube ω:

$$q=\frac{q_m}{h},\quad u=\frac{u_a}{h}\frac{2S_t}{S_m},\quad \tau=\omega t\quad\text{with }\omega=\frac{c_0\pi}{L}. \tag{21}$$

Inserting these quantities into Eqs. (6) and (15), taking (18) and (19) into account, we finally obtain the following non-dimensional two dof system:

$$\frac{\mathrm{d}^2u}{\mathrm{d}\tau^2}+\lambda\frac{\mathrm{d}u}{\mathrm{d}\tau}+u+\beta(u-q)=F\cos\left(\frac{\Omega}{\omega}\tau\right),$$

$$\gamma\frac{\mathrm{d}^2q}{\mathrm{d}\tau^2}+c_1\left[\left(\frac{f_1}{f_0}\right)^2q+\eta\omega\frac{\mathrm{d}q}{\mathrm{d}\tau}\right]+c_3\left(2\eta\omega q^2\frac{\mathrm{d}q}{\mathrm{d}\tau}+q^3\right)=\beta(u-q), \tag{22}$$

where

$$\beta=\frac{2S_tL}{V_2\pi^2},\quad \lambda=\frac{2c_f}{\rho_aS_tc_0\pi},\quad \gamma=\frac{8}{3}\frac{\rho_mhS_t}{\rho_aLS_m},$$

$$c_1=\frac{2*1.015^4\pi}{9(1-\nu^2)}\frac{Eh^3LS_t}{\rho_ac_0^2R^6},\quad c_3=\frac{64}{3\pi^3(1-\nu^2)}\frac{Eh^3LS_t}{\rho_ac_0^2R^6},$$

$$f_0=\frac{1}{2\pi}\sqrt{\frac{1.015^4\pi^4Eh^2}{12(1-\nu^2)\rho_mR^4}}. \tag{23}$$

This system differs from (1) on the following points:

- the nonlinear absorber does not show a pure cubic stiffness response. The normalized pre-stress χ applied to the membrane introduces a linear contribution.
- there are two damping terms in the equation for the nonlinear oscillator. The main term is the nonlinear contribution $2c_3\eta\omega q^2\mathrm{d}q/\mathrm{d}\tau$ which corresponds to a viscous dissipation at large vibration amplitude.

Despite these differences, this system is able to clearly reproduce the targeted energy transfer when the χ parameter is not too large, the parameter γ is equal to approximately unity and the coupling β is around 0.1.

2.3.6. Nonlinear normal modes

It has been shown that the energy pumping phenomenon is caused by a 1:1 resonance capture [8]. This can be enlightened by looking at the nonlinear normal modes of the system (here we use the same notations as [45]). Using the harmonic balance method, we express the motion in the form $u_a(t)=U\cos(\omega t)$ and $q_m(t)=Q\cos(\omega t)$. Introducing it into the system (20) without the damping terms, with F=0 and neglecting the higher harmonics, we obtain the following algebraic system for the amplitudes U and Q:

$$(-m_a\omega^2+k_a+S_t^2k_b)U-S_t\frac{S_m}{2}k_bQ=0,$$

$$\left(-m_m\omega^2+k_1\left(\frac{f_1}{f_0}\right)^2+\left(\frac{S_m}{2}\right)^2k_b\right)Q-S_t\frac{S_m}{2}k_bU-\frac{3}{4}k_3Q^3=0. \tag{24}$$

This system can be easily solved in closed form and the curves of the solutions $U(\omega)$ and $Q(\omega)$ calculated with the configuration h=0.6, R=30 mm, f_1 = 57 Hz are reported in Fig. 5. As the motions of the two oscillators are assumed to be synchronous on the same frequency (1:1 resonance capture), we call the solution where $u_a(t)$ and $q_m(t)$ are out of phase the nonlinear normal mode (NNM) S11−, and the solution where $u_a(t)$ and $q_m(t)$ are in phase the NNM S11+. Based on the previous model, the energy E of the global system can be defined as follows:

$$E(\omega)=\frac{1}{2}k_aU(\omega)^2+\frac{1}{2}k_1\left(\frac{f_1}{f_0}\right)^2Q(\omega)^2+\frac{1}{4}k_3Q(\omega)^4+\frac{1}{2}k_b\left(S_tU(\omega)-\frac{S_m}{2}Q(\omega)\right)^2. \tag{25}$$

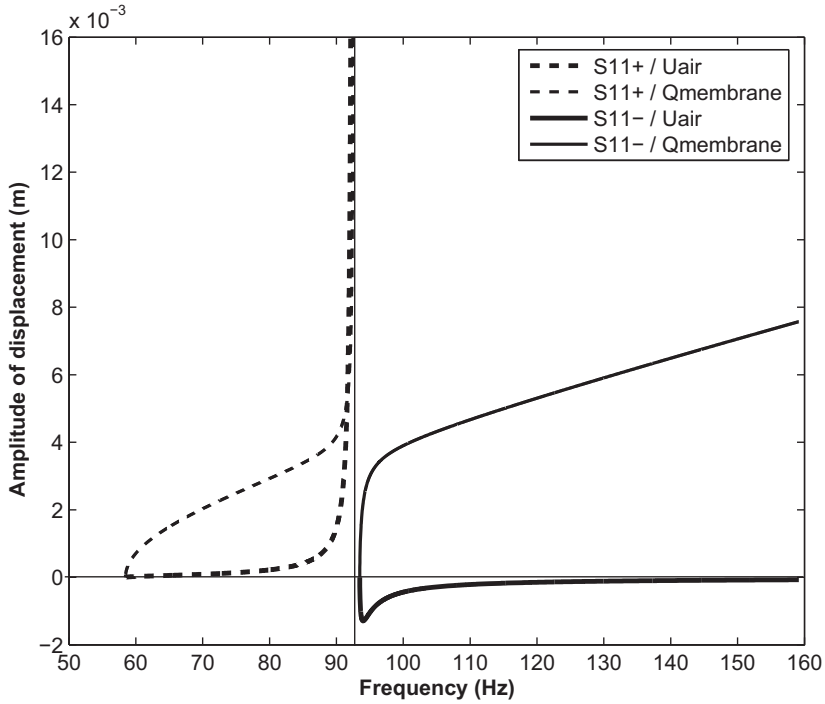

Fig. 5. Nonlinear normal modes of the system—amplitudes.

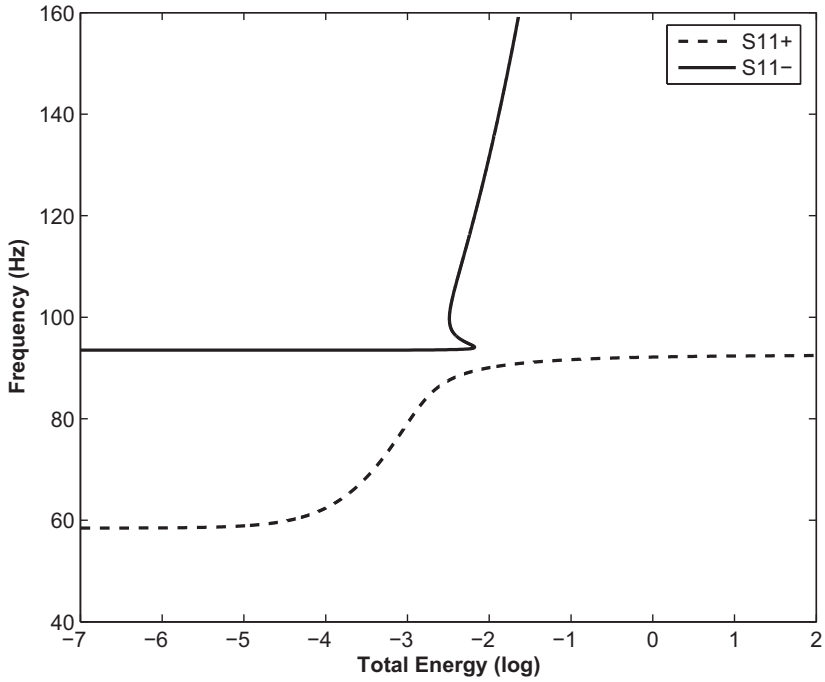

Fig. 6. Nonlinear normal modes of the system—frequency–energy plot.

The frequency–energy plot (Fig. 6) is then obtained by plotting the frequency versus the energy E with a log scale. The two different NNMs S11− and S11+ and their coincidence for the low energies with the linear modes of the tube (horizontal line at 92 Hz) and the membrane (horizontal line at 57 Hz) can be clearly seen in this figure. As we will see later on, this frequency–energy plot is very useful to understand the energy pumping mechanism.

2.4. Experimental verification of the cubic stiffness of the membrane

The second experimental set-up shown in Fig. 7 has been developed to characterize the stiffness of the membrane. In the aim to measure the quasi-static relation between the pressure and the displacement of the membrane, we have connected its attachment device on an airtight cavity. Thanks to an air pump, the static pressure inside the cavity could be increased. The difference of the pressure inside and outside of the cavity is measured thanks to a differential pressure sensor. A laser triangulation sensor measures the displacement of the center of the membrane (see Fig. 8).

Fig. 9 shows the amplitude response of the membrane (configuration h=0.18, R=40 mm) when the static pressure is varying with three different pre-stresses. We clearly see that the stiffness is nonlinear, with a contribution depending on the pre-stress. A cubic polynomial fit of the curves of Fig. 9 from the smallest to the strongest pre-stress gives the results: $(S_m/2)p = 51.55q_m + 6.19 \times 10^5 q_m^3$, $(S_m/2)p = 68.65q_m + 6.23 \times 10^5 q_m^3$, $(S_m/2)p = 95.80q_m + 5.87 \times 10^5 q_m^3$. For this configuration, the value of the parameter k_3 (from the expression (16)) is $1.76 \times 10^6\,\mathrm{N\,m^{-3}}$. Qualitatively, the pre-stress mostly affects the linear part of the stiffness, while the cubic one remains almost constant. This behaviour is the one expected from Eq. (15). Quantitatively, the theoretical value of k_3 is three times the experimental one. This is not too surprising since it is well known that a one dof reduced model is more stiff than the continuous model it comes from. However, a comparison of the one dof model and a finite element plate simulation shows only a ratio of two on the value of k_3. The remaining difference can be explained by two other factors: first we compare a dynamical model with a static experiment and second great uncertainties exist for the values of h, E and ν which can vary the value of k_3 of ± 30 percent. As we could not measure the tension or the first natural frequency of the membrane on this set-up, the associated value of the parameter k_1 cannot be calculated.

3. Regimes observed experimentally under sinusoidal excitation

In Figs. 10, 11, 14–16 the first channel is the signal of the sinusoidal forcing sent to the loudspeaker, the second channel is the acoustic pressure measured at the center of the tube and the third channel is the velocity of the center of the membrane.

In this part, we focus on the behaviour of the system under sinusoidal excitation, at the frequency of the first acoustic mode of the tube and with the set-up configuration: L=2 m, h=0.4, R=30 mm, f_1=62 Hz. Due to the presence of a nonlinearity, several types of behaviour are observed, depending on the level of the excitation.

When the excitation level is below a certain threshold S_1, the regime observed is periodic (Fig. 10) and the vibration energy is localized on the tube where the sound level is important whereas the membrane is inactive and has small vibrations. Fig. 12(a) is simply a zoom of part of Fig. 10 showing the phases of the signals, and the same recording is presented in Fig. 13(a) but in terms of displacements. To shift from the velocity $\dot{q}_m$ of the membrane to its displacement q_m, a simple integration is computed. And to shift from the acoustic pressure p at the center of the tube to the displacement u_a of the air at the end of the tube (z=L), we use the relation between amplitudes u_0 and p_0 presented above $u_0 = p_0 L/\rho_a c_0^2 \pi$ and the fact that u_a and p are necessarily out of phase on the first acoustic mode of the tube. The relation between u_a and p is therefore $u_a(L,t) = -p(L/2,t)L/\rho_a c_0^2 \pi$. It can thus be seen that, in this regime, the displacement of the air at the end of the tube u_a and the displacement of the center of the membrane q_m are synchronous at the same frequency and almost out of phase. The system is therefore on the neighbourhood of the so-called nonlinear normal mode S11 $-$. If the excitation level is higher than a second threshold S_2 ($S_2 > S_1$), the regime will also be periodic but the energy will be localized in the

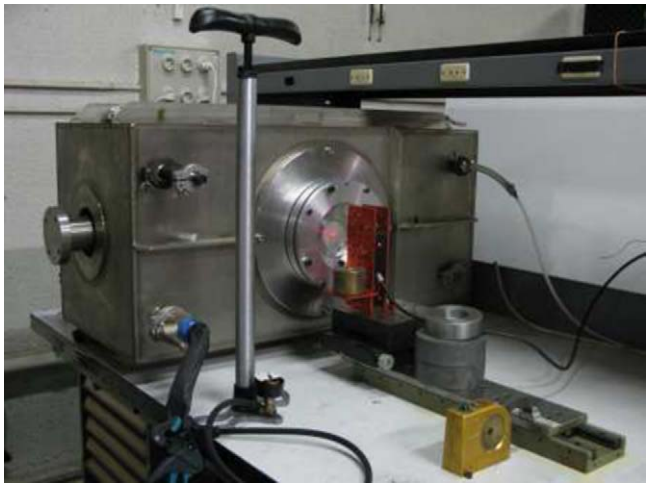

Fig. 7. Picture of the experimental set-up used to characterize the membrane.

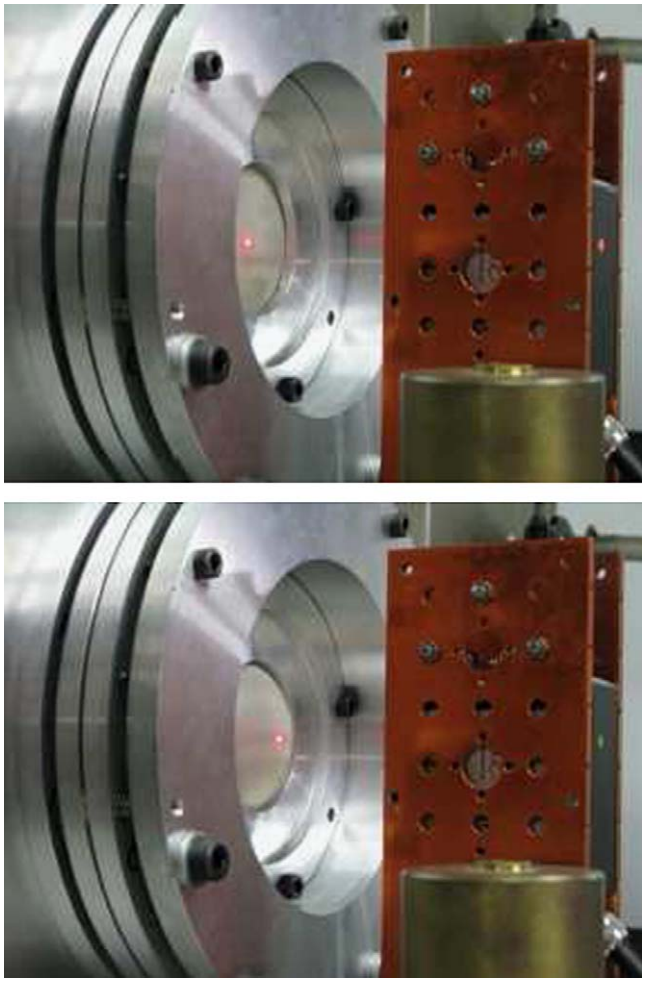

Fig. 8. Picture of the membrane without (top) and with pressure (bottom).

membrane which vibrates with large amplitudes (Figs. 11 and 12(b)). As can be seen from Fig. 13(b), u_a and q_m are still synchronous at the same frequency, but they are now almost in phase. This regime corresponds therefore to a point in the neighbourhood of S11+. Between these two thresholds, the regime is nearly periodic (almost quasi-periodic) with a slow evolution of the amplitudes of both oscillators. We can see in Fig. 14 that the amplitude of the pressure at the middle of the tube increases and decreases repeatedly in a regular fashion. For the amplitude of the membrane, we can distinguish roughly two levels: a small one corresponding to the growth of the pressure, and a bigger one when the pressure amplitude decreases. This alternating regime is referred to as a strongly modulated response in Chapter 6 of [32] where a detailed analysis of the phenomenon is proposed, see also [46,47]. When the pressure in the tube decreases, the membrane performs almost constant amplitude oscillations. The situation is here very similar to the one for free vibrations (Section 4) where a quasi-irreversible transfer of energy occurs from the acoustic medium to the membrane. When the level of the pressure gets below a threshold, the transfer is stopped and the pressure amplitude increases again.

4. Free oscillations observed experimentally

Since the energy pumping is an intrinsically transient phenomenon, this part deals with the behaviour of the system under free oscillations with the configuration: $L=2$ m, $h=0.6$, $R=30$ mm, $f_1=57$ Hz. Practically, a sinusoidal excitation at the first resonance frequency of the tube is applied in order to put enough energy in the system. This excitation is suddenly stopped, and then on, we observe the free oscillations of the system. Several illustrations are given in this part showing the two different types of behaviour observed depending on the initial conditions.

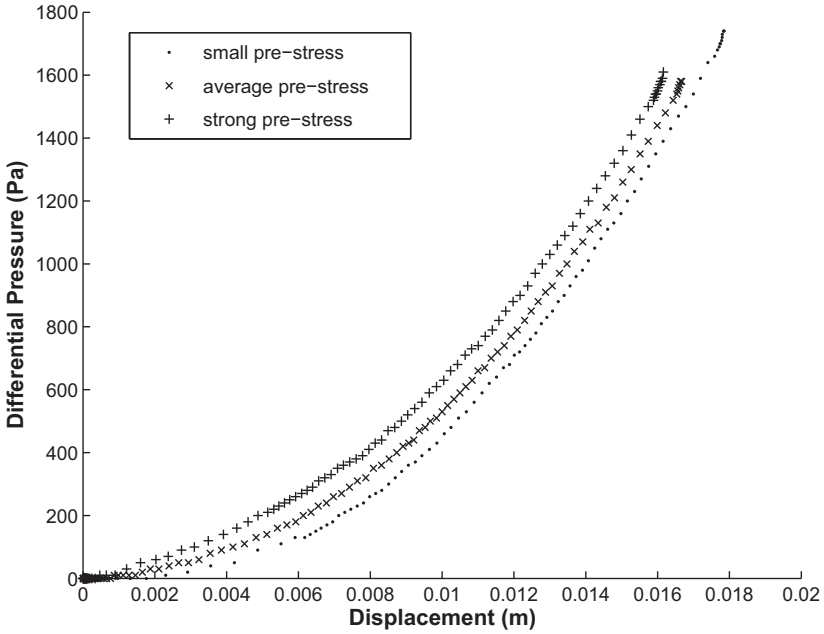

Fig. 9. *Experimental result*. Relation between differential pressure and displacement of the membrane for three different pre-stresses.

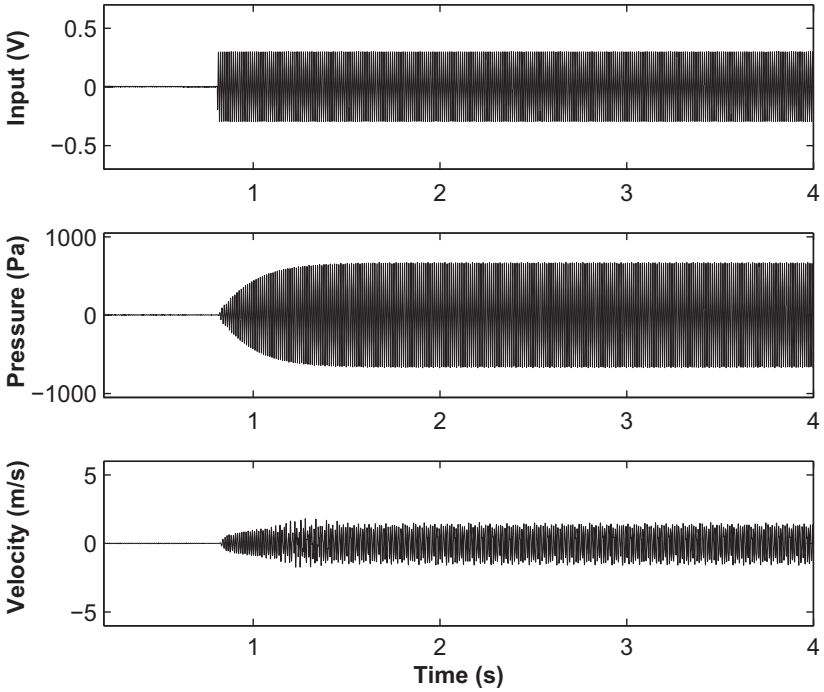

Fig. 10. *Experimental result*. Low excitation amplitude: periodic regime in the neighbourhood of S11− localized on the tube. Input voltage: $\mathcal{A} = 0.29\,\mathrm{V}$.

4.1. Time series

If at the initial instant of the free oscillations, the system vibrates close to S11− (low excitation amplitude: $\mathcal{A} = 0.5\,\mathrm{V}$), then the sound extinction in the tube will follow a natural exponential decrease (Fig. 15) and the NES will be inactive. But if at the initial instant, the system vibrates close to S11+ (high excitation amplitude: $\mathcal{A} = 3.7\,\mathrm{V}$), then the sound extinction in the tube will follow a quasi-linear decrease, much faster than the exponential one, during which the membrane will still vibrate with a large amplitude until the sound in the tube has been almost completely cancelled (Fig. 16). During this

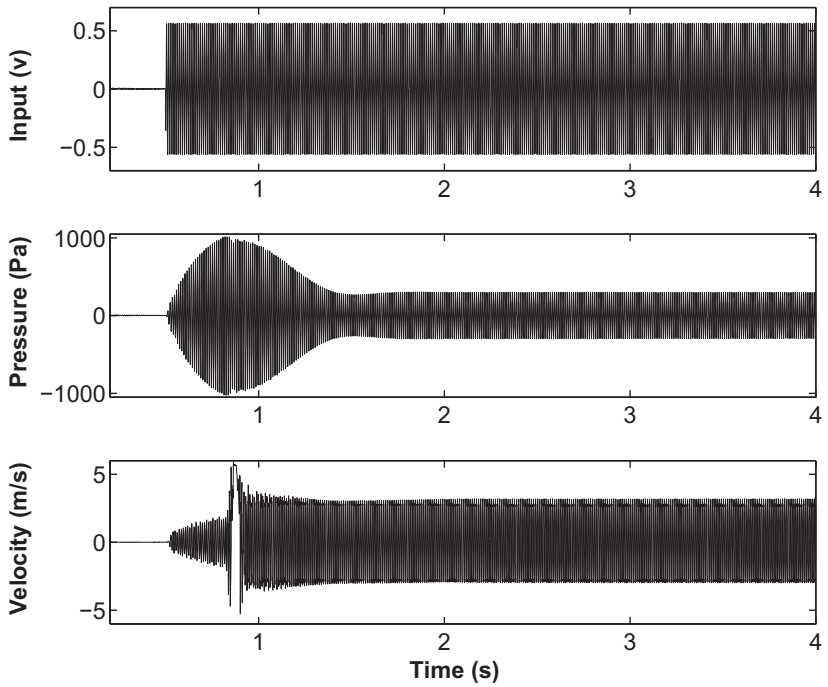

Fig. 11. *Experimental result*. High excitation amplitude: periodic regime in the neighbourhood of S11+ localized on the membrane. Input voltage: $\mathcal{A} = 0.59\,\mathrm{V}$.

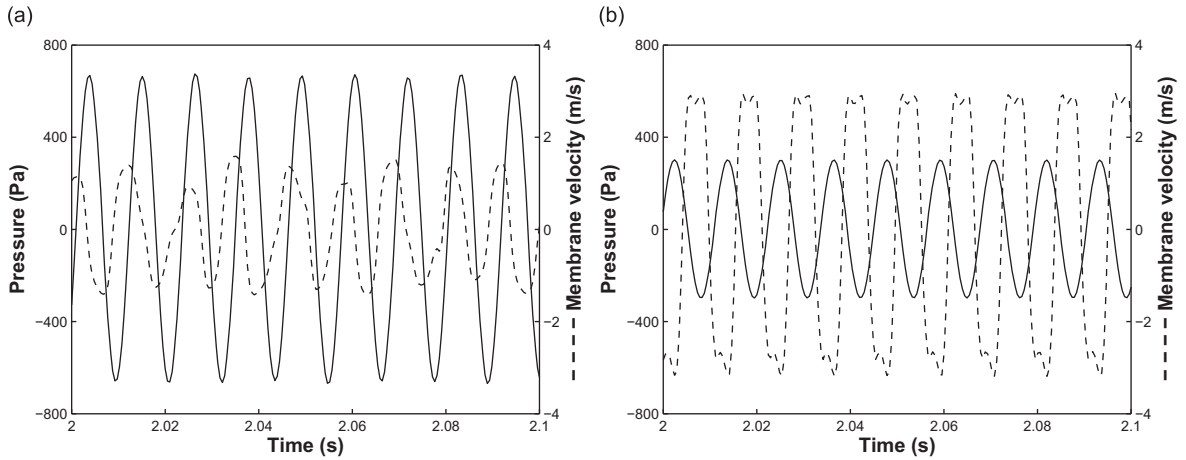

Fig. 12. *Experimental result*. Zoom onto Figs. 10 (12(a)) and 11 (12(b)) showing shape and phase of membrane velocity and acoustic pressure signals.

phase, an irreversible energy transfer occurs from the tube to the membrane: the NES quickly captures the resonance of the tube, localizes the energy of the acoustic medium and then damps it by viscosity in the membrane as well as by acoustic radiation outside the set-up. From an analysis of the resonance bandwidths of the membrane, which is experimentally measured with a low broadband excitation, we could quantify the sum of viscous damping and acoustic radiation damping. On the other hand, we quantify the acoustic radiation damping of the membrane using the approach given in [48]. The result is that the viscous damping is around 10 times larger than the acoustic radiation damping. The energy which has been localized in the membrane is then mainly damped by viscosity. Note that, for this configuration, the excitation thresholds S_1 and S_2 are around 1.8 and 2.2 V, respectively.

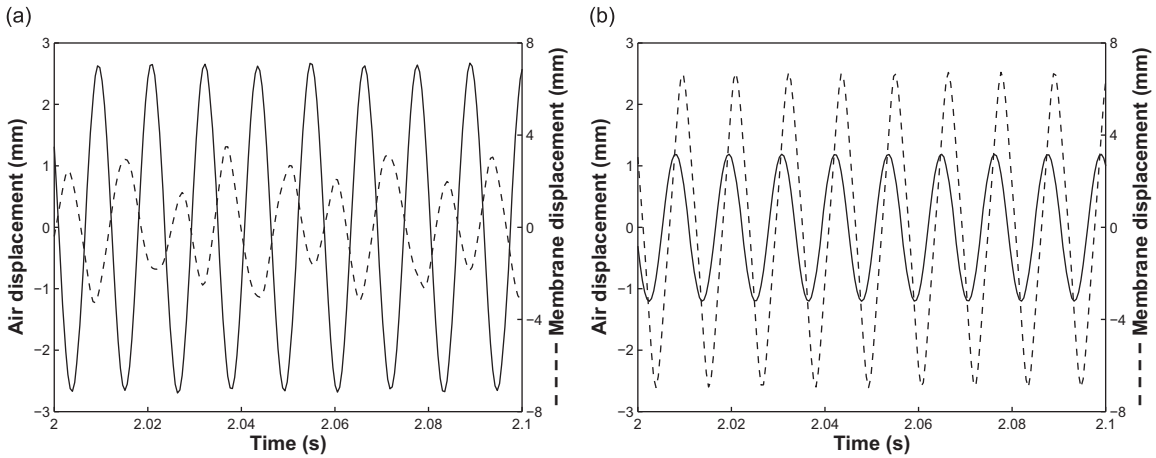

Fig. 13. *Experimental result*. Plot of the times series shown in Fig. 12 showing shape and phase of the signals but in terms of displacements (displacement of the air at the end of the tube and displacement of the center of the membrane). (a) A point in the neighbourhood of S11 − : localization on the tube and signals almost out of phase. (b) A point in the neighbourhood of S11+: localization on the membrane and signals almost in phase.

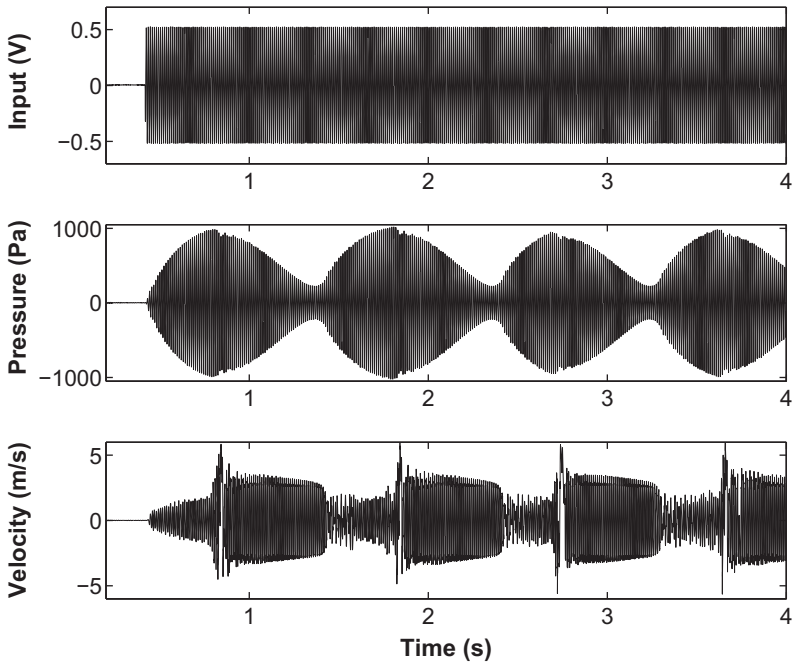

Fig. 14. *Experimental result*. Intermediate excitation amplitude: quasi-periodic regime. Input voltage: $\mathcal{A} = 0.51$ V.

4.2. Evolution of the energy of the system

Thanks to the model presented above, we can define and compute the energy of the different elements of the system:

$$E_{\text{tube}} = \frac{1}{2} m_a \dot{u}_a^2 + \tfrac{1}{2} k_a u_a^2,$$

$$E_{\text{membrane}} = \frac{1}{2} m_m \dot{q}_m^2 + \tfrac{1}{4} k_3 q_m^4,$$

$$E_{\text{coupling box}} = \frac{1}{2} k_b \left(S_t u_a - \frac{S_m}{2} q_m \right)^2,$$

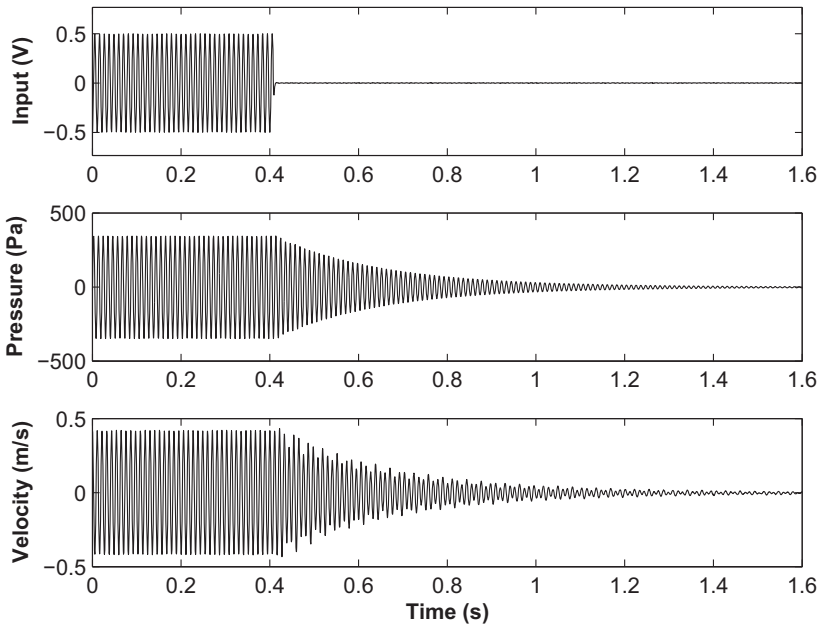

Fig. 15. *Experimental result*. Free oscillations with initial conditions close to S11− (low input voltage: $\mathcal{A}=0.5\,\mathrm{V}$): observation of an exponential decrease for the acoustic pressure.

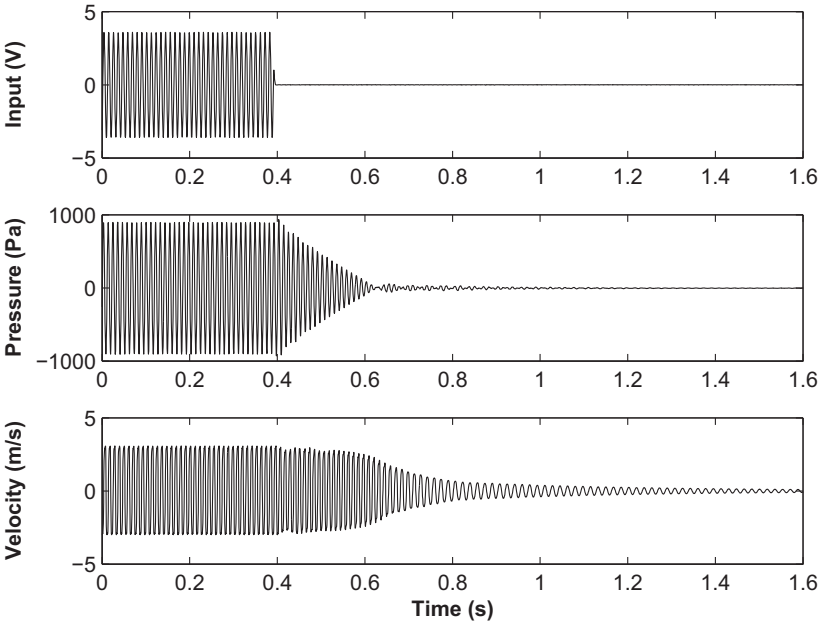

Fig. 16. *Experimental result*. Free oscillations with initial conditions close to S11+ (high input voltage: $\mathcal{A}=3.7\,\mathrm{V}$): observation of a quasi-linear decrease for the acoustic pressure.

$$E_{\mathrm{total}}=E_{\mathrm{tube}}+E_{\mathrm{membrane}}+E_{\mathrm{coupling\ box}}. \tag{26}$$

Figs. 17 and 18 show the evolution of the energy and the percentage of the energy present in the tube and in the membrane, which was computed from the time series given in Figs. 15 and 16. It appears clearly that in the first case (Fig. 17) the energy always remains localized in the tube whereas the membrane is never active. But in the second case (Fig. 18), the energy is entirely transferred to the membrane which localizes quickly almost 100 percent of the energy of the system.

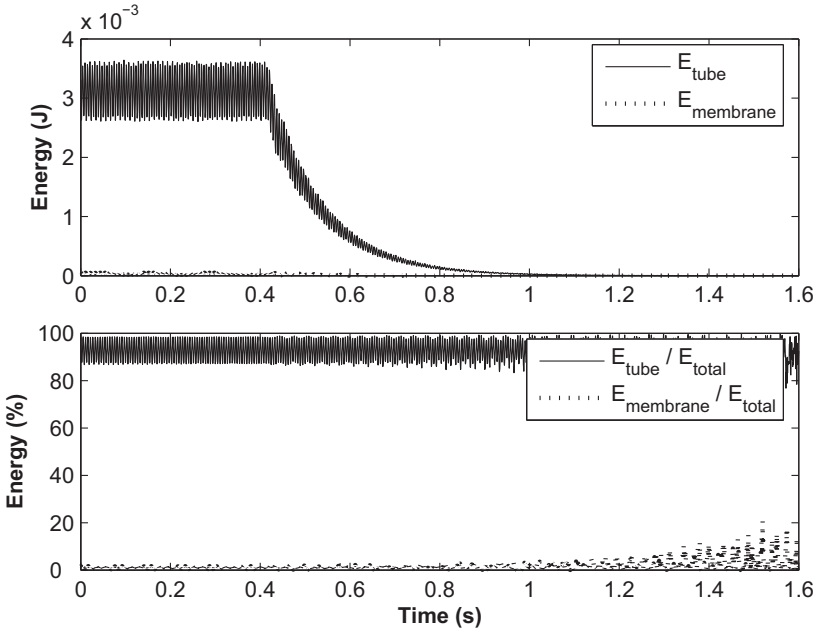

Fig. 17. *Experimental result*. Evolution of the energy in the tube and the membrane for the time series shown in Fig. 15 (low input voltage: $\mathcal{A} = 0.5\,\mathrm{V}$).

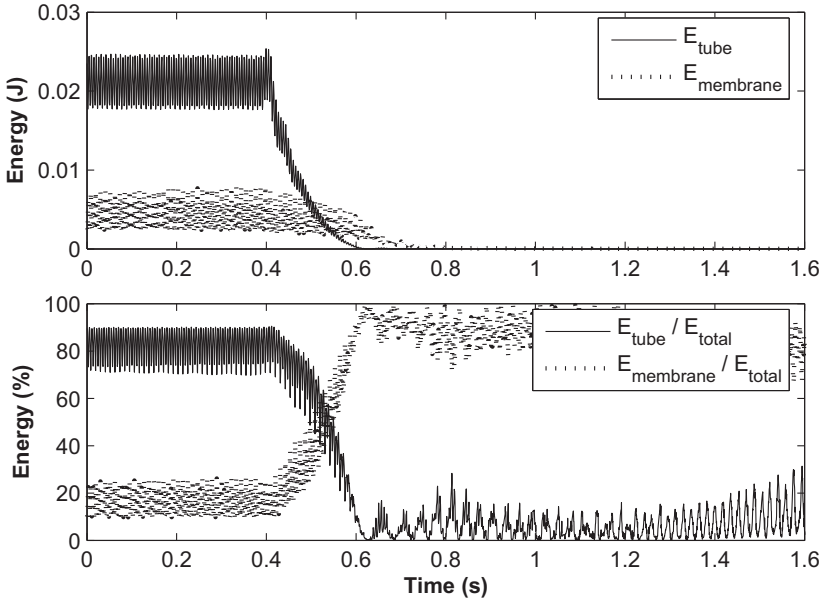

Fig. 18. *Experimental result*. Evolution of the energy in the tube and the membrane for the time series shown in Fig. 16 (high input voltage: $\mathcal{A} = 3.7\,\mathrm{V}$).

4.3. Wavelet transform

The wavelet transform of the same time series gives another illustration about the evolution of the frequency content of these signals. As can be seen in Figs. 19 and 20, the excitation in both cases is a single frequency signal on the resonance frequency of the tube. Only the level is different. In Fig. 19 (initial conditions close to S11 −), the frequency of the other two time series can be seen to remain constant at that resonance frequency, nothing worth noting occurs. On the other hand, if the initial condition is close to S11+, we can see in Fig. 20 that the acoustic pressure is quickly cancelled and from then on, the frequency of the membrane drops down together with its energy (which is a characteristic of a cubic oscillator), leaving the 1:1 resonance capture and then avoiding the return of the energy. Actually, this frequency decreases until it reaches the first linear resonance frequency of the membrane, which in this case is 57 Hz.

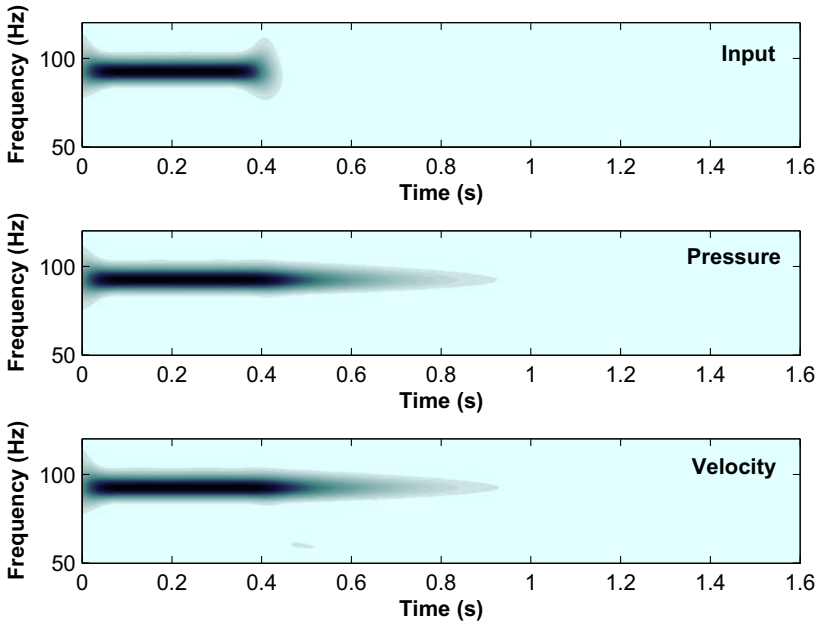

Fig. 19. *Experimental result*. Wavelet transform of the time series shown in Fig. 15 (low input voltage: $\mathcal{A} = 0.5\,\mathrm{V}$).

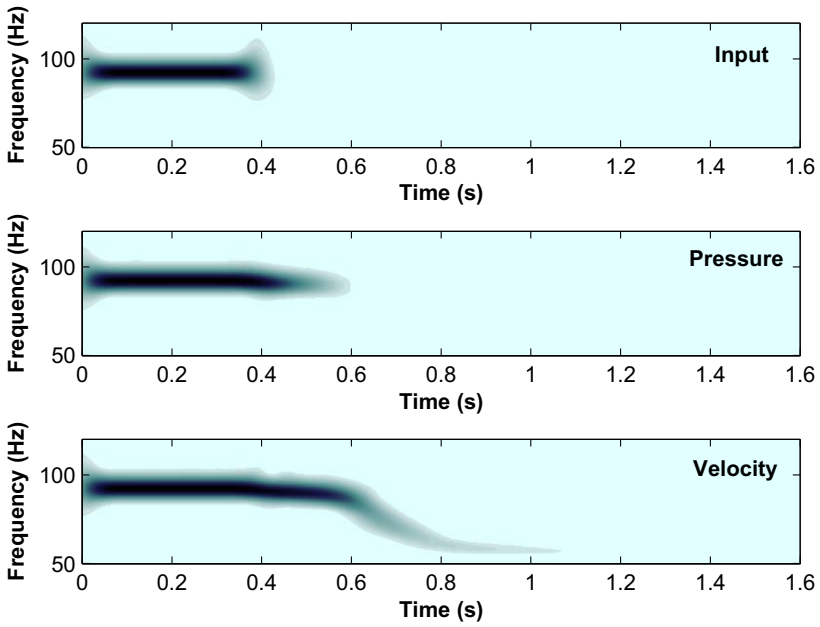

Fig. 20. *Experimental result*. Wavelet transform of the time series shown in Fig. 16 (high input voltage: $\mathcal{A} = 3.7\,\mathrm{V}$).

4.4. Frequency–energy plots

Computing the evolution of the total energy of the system E_{total} and replacing the time axis by this total energy in the previous frequency–time plot of Figs. 19 and 20, we can plot the frequency–energy plot corresponding to the experimental time series. Superposing it on the nonlinear normal modes, we can clearly see which way is followed by the system. In the first case (Fig. 21) where the system is initially close to S11− (which is clearly visible here), the extinction follows this mode towards the low energy side. But in the second case (Fig. 22), the system is initially close to S11+ and then keeps strictly to this mode until the energy has been completely cancelled. All the differences between the two mechanisms observed here are due to the fact that the system follows one NNM or the other.

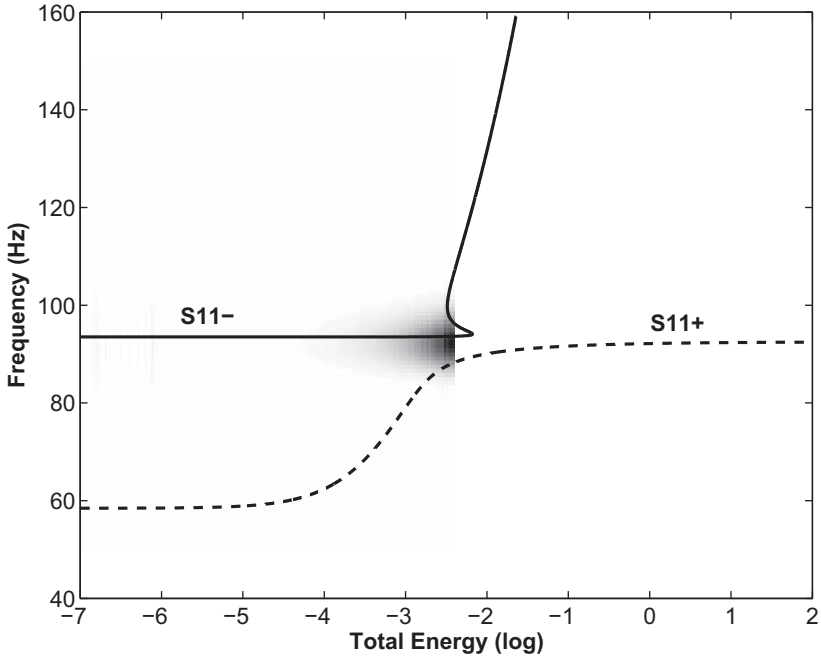

Fig. 21. *Experimental and numerical results*. Frequency–energy plot of the pressure time series shown in Fig. 15 (low input voltage: $\mathcal{A} = 0.5\,\mathrm{V}$) and nonlinear normal modes of the system.

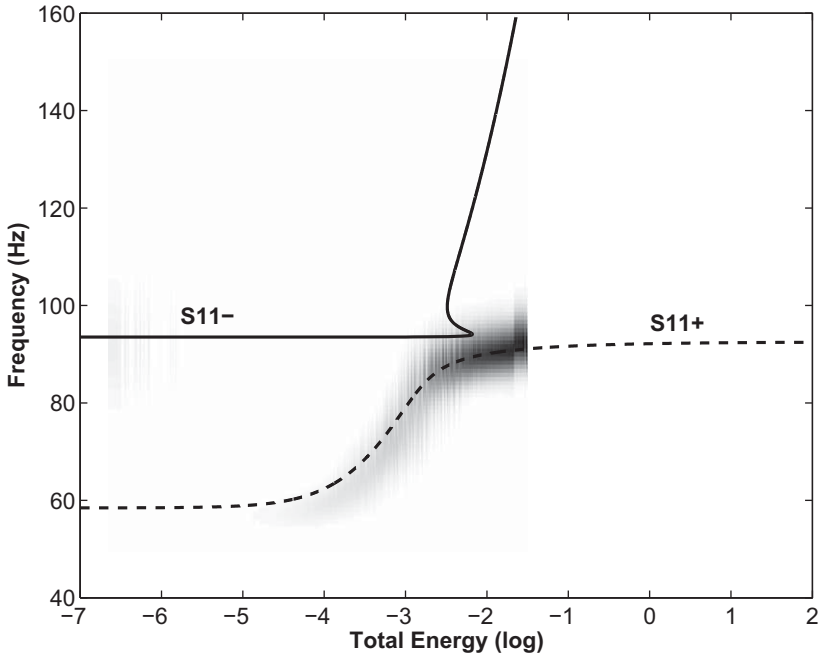

Fig. 22. *Experimental and numerical results*. Frequency–energy plot of the velocity time series shown in Fig. 16 (low input voltage: $\mathcal{A} = 3.7\,\mathrm{V}$) and nonlinear normal modes of the system.

5. Comparison between experimental and numerical results

Numerical simulations of free oscillations have been made from the model presented in Section 2. The parameters used for these simulations were exactly the physical parameters of the set-up. Each of them has been measured excepted the damping factor η of the membrane. Only the value of that parameter has been fitted numerically in order to obtain the best

match with the measurements. For each membrane used, the damping factor has been identified in this way, leading to values in the range 10^{-3}–10^{-4}.

Despite of the very important acoustic levels that we have measured in the tube, the experimental set-up has been designed so that most of nonlinear phenomena occur in the membrane, and are prevented in the source and the acoustic resonator. This can be checked from the maximum value $p_{\max}$ of the pressure inside the resonator : it reaches about 1000 Pa, leading to a velocity $v_{\max}$ of about 2.5 m s^{-1} at each end of the tube. Thus, the adimensional factors $p_{\max}/P_{\text{atm}}$ and $v_{\max}/c_0$ are both below 10^{-2}, ensuring that the linear acoustic assumption is valid. The main nonlinearity source could, however, be the generation of "mushroom-shaped" vortices at the end of the tube. For a cylindrical port, previous work [49] has shown that these must be considered as significant for velocities over about 10 m s^{-1}. This has also been checked by local measurements [50] which showed that indeed vortices may appear around a few m s^{-1} if the tube edges are sharp, but that they remain localized close to these edges: the average velocity is therefore only marginally impacted by these vortices (especially considering the relatively large area of our tube). Lastly, the loudspeaker itself has been selected so that the membrane displacement which is required to reach the necessary level is within the linear displacement stated by the manufacturer. It has then been checked that the pressure inside the coupling volume on the loudspeaker side does not reflect a dramatic harmonic distortion.

Figs. 23 and 24 show the comparison between simulations and measurements of the free oscillations of the system after a sinusoidal excitation at the resonance frequency of the tube. The first case corresponds to the following experimental set-up: $\mathcal{A}=1$ V, R=20 mm, h=0.39 mm, $\eta=0.00062$ s, $f_1=62$ Hz, $L=2$ m. The values of the other fixed parameters are: c_0=350 m s^{-1}, R_t=47 mm, V_2=27 $\times$ 10^{-3} m^3, $\lambda=0.014$, $\rho_m=980$ kg m^{-3}, $\rho_a=1.3$ kg m^{-3}, E=1.48 MPa, $\nu=0.49$. The second case corresponds to a configuration with the same membrane but with a stronger initial excitation, a larger radius and a different pre-stress: $\mathcal{A}=3$ V, R=30 mm, f_1=73 Hz. In each case, the simulations were calculated adjusting the amplitude of the input so that the amplitude of the initial numerical acoustic pressure is equal to the initial measured one. The input is then reduced to zero at the instant when the experimental input signal is cut. We observe then that the simulations provide a very good match with the measurements in both cases, especially for the acoustic pressure. The changes in the behaviour of the system, induced by a different membrane radius and pre-stress, are accurately accounted for by the model. In the case of the membrane velocity, the simulation gives in both cases the same global behaviour but with smaller amplitude than the measured one. These results are fairly satisfactory, especially considering the rough approximations that have been made in the modelling of the membrane. Our studies have shown that the numerical simulations, with any other values of parameters (radius, pre-stress, thickness of the membrane, length of the tube, etc.), always follow the experimental results with a similar level of accuracy as in the case of these two examples. That is to say that the behaviour changes, induced by any change of parameter, observed numerically are in perfect agreement with those observed experimentally.

6. Frequency aspects of energy pumping

In Section 3, we have presented the behaviour of the system under a sinusoidal forcing with a fixed frequency and a varying amplitude. In Section 4, we have discussed the free vibration behaviour. Now let us look at the behaviour of that acoustic medium coupled to a membrane when the frequency of the sinusoidal forcing varies. Because of the presence of

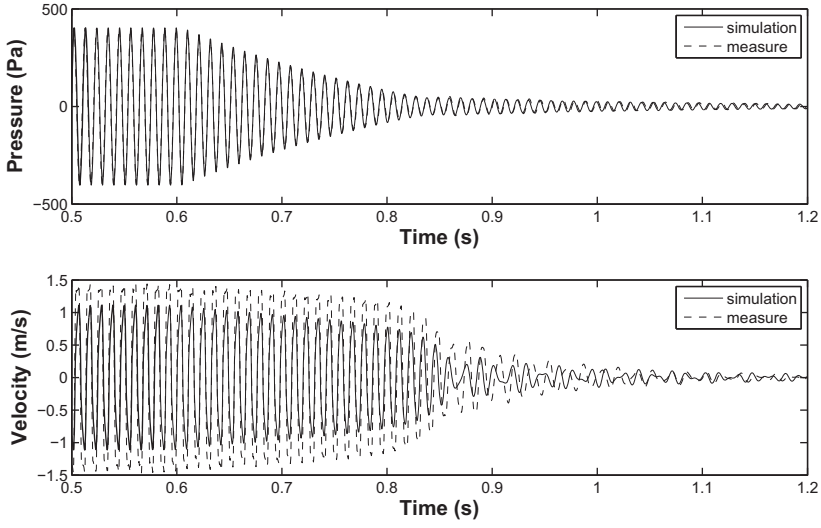

Fig. 23. *Experimental and numerical results*. Comparison of the free oscillations between experimental data and simulations. Configuration 1: $\mathcal{A}=1$ V, h=0.39 mm, R=20 mm, f_1=62 Hz.

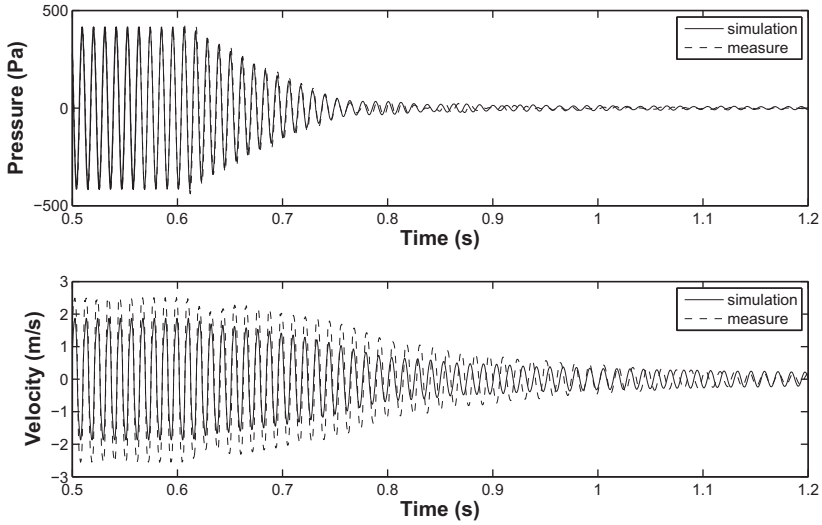

Fig. 24. *Experimental and numerical results*. Comparison of the free oscillations between experimental data and simulations. Configuration 2: $\mathcal{A}=3$ V, h=0.39 mm, R=30 mm, f_1 = 73 Hz.

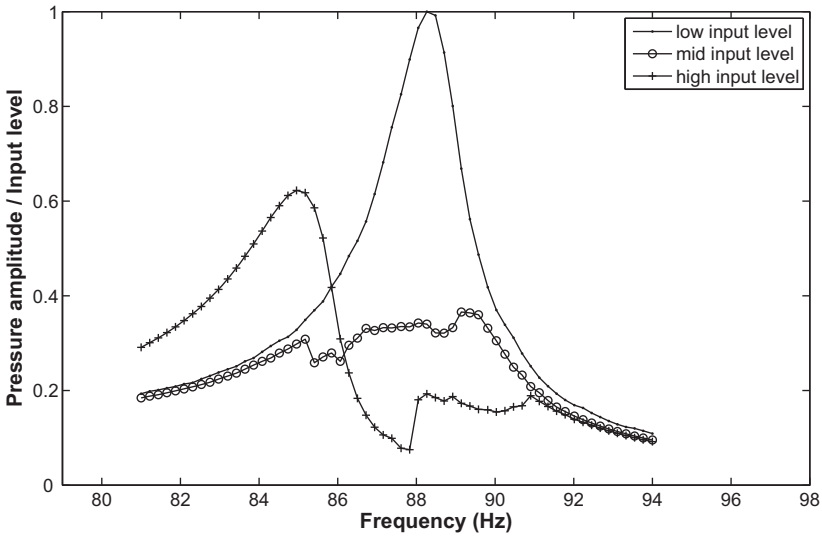

Fig. 25. *Experimental result*. Three different kinds of frequency responses depending on the excitation amplitude. Low amplitude: resonance peak of the tube; intermediate amplitude: energy pumping and clipping of the peak; high amplitude: a different but lower resonance peak. Configuration: L=2.22 m, h=0.18 mm, R=40 mm, f_1 = 45 Hz.

a nonlinearity, we cannot talk about transfer function as the behaviour of the system depends on the amplitude of excitation. Indeed as we see in Fig. 25, there are several kinds of frequency responses. The set-up configuration here is: L=2.22 m, h=0.18, R=40 mm, f_1=45 Hz. This figure shows the experimental normalized values of the amplitude of the acoustic pressure in the tube divided by the amplitude of excitation during constant amplitude frequency sweeps. When the level of excitation is lower than S_1, the membrane remains inactive during the entire sweep and the system has only the resonance peak of the tube without membrane (when the membrane is occulted, the peak does not change). For a level between S_1 and S_2, a clipping of the peak appears. For frequencies below 85.5 Hz and above 89.5 Hz the sound level in the tube is too low to activate the energy pumping and the frequency response is identical to that obtained for low levels. But in between those frequencies, i.e. close to the acoustic resonance of the linear system, the level increases enough to set the system on the quasi-periodic regime corresponding to the energy pumping and that creates a clipping of the peak. In that frequency range, energy pumping prevents sound pressure from exceeding a certain level. When the excitation level is higher than S_2, the system has a frequency response with a new resonance peak. The resonance frequency of this peak is smaller than the resonance frequency of the tube and the maximal amplitude is slightly lower than the maximal amplitude of the resonance peak of the tube. Below 87.5 Hz, the vibration regime is periodic and the membrane is activated, vibrating

in phase with the acoustic displacement. Between 87.5 and 91 Hz, the regime is quasi-periodic. And above 91 Hz, the regime is also periodic, but the membrane is not activated, and the three curves are then combined. In a noise reduction context, this frequency response is obviously much less interesting than the clipping peak produced by energy pumping, but as we can see, that phenomenon cannot appear with too strong levels. Simulations of frequency responses have been done from our model with the same configuration than experimentally. As we can see in Fig. 26, the three kinds of frequency responses are also obtained with a correct correlation with experimental results.

Now, for the same set-up configuration, the frequency response is presented under the form of a surface, the practical expression of energy pumping appears clearly as a level limitation. Fig. 27 shows the experimental results of successive frequency sweeps under a large span of excitation levels. The results are presented under the form of a surface level of acoustic pressure depending on the frequency and the excitation level. We recognize in the low excitation zone the

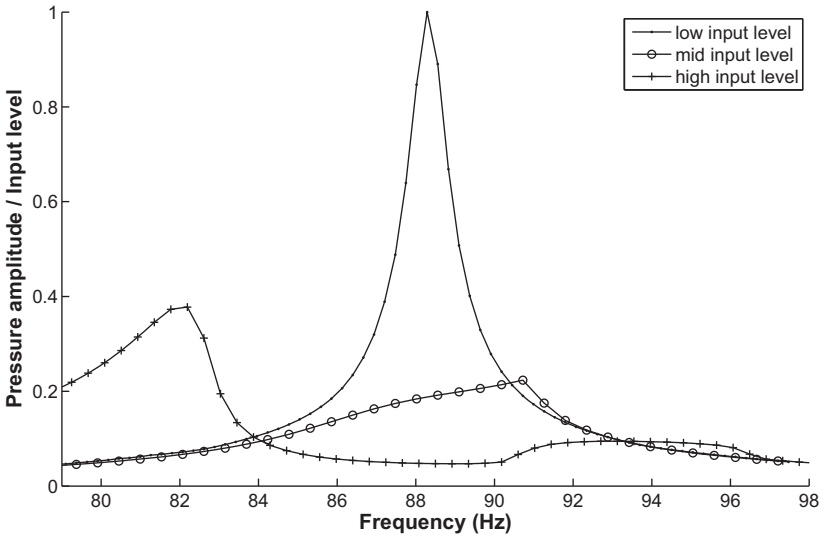

Fig. 26. *Numerical result*. Simulations of frequency responses for the same configuration and observation of the same three kinds of responses (cf. Fig. 25).

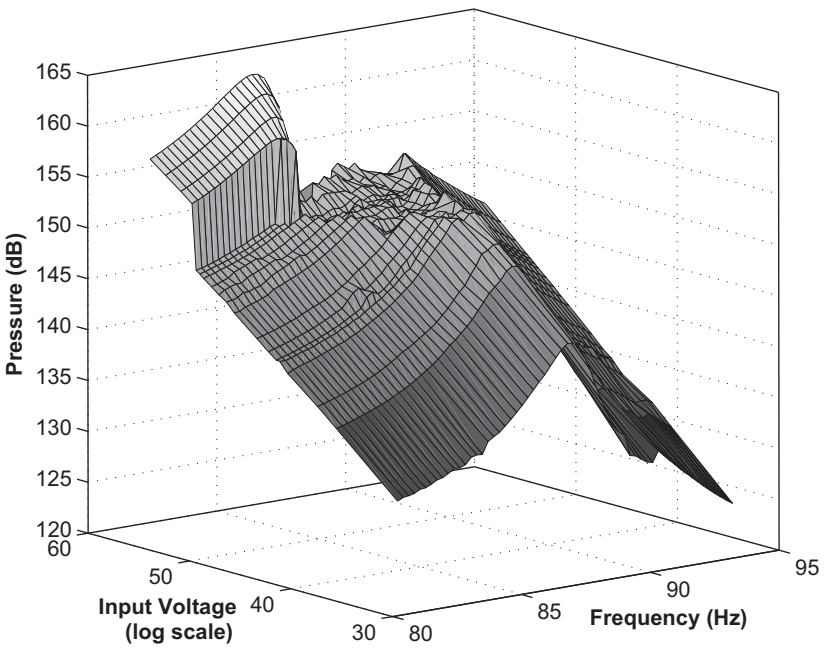

Fig. 27. *Experimental result*. Surface representation of experimental frequency responses: observation of the sound limitation ceiling in the energy pumping zone. Configuration: L=2.22 m, h=0.18, R=40 mm, f_1=45 Hz.

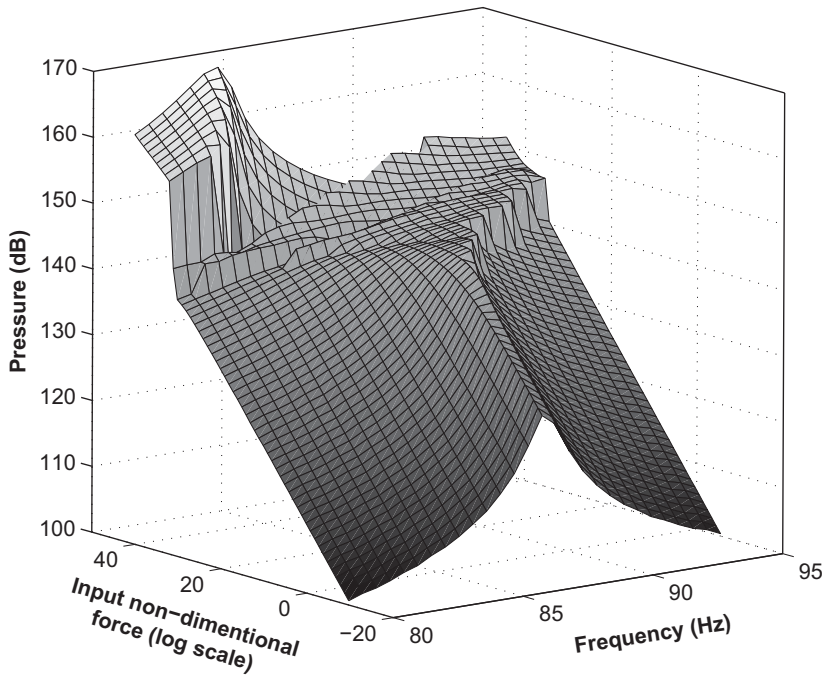

Fig. 28. *Numerical result*. Simulation of the surface representation of frequency responses for the same configuration: observation of the same sound limitation ceiling in the energy pumping zone (cf. Fig. 27).

resonance peak of the tube. Naturally in this zone, the higher the excitation level, the higher the level of the peak. Between excitation thresholds S_1 and S_2, a clipping of the top of the peak appears, and the sound level in the tube cannot exceed a certain ceiling which is here around 150 dB. In this zone, when the level of excitation increases, the clipping of the peak becomes larger and the sound level remains limited at the same maximum. The energy pumping acts then on the acoustic medium as a level limitation. Above the excitation threshold S_2, clipping is changed into a resonance peak slightly shifted to low frequencies. This figure clearly shows an important property of energy pumping: it only exists inside a limited range of excitation levels. The simulation of the surface has also been computed from the model (Fig. 28) and it shows a very similar shape with a energy pumping ceiling which is a little lower (between 140 and 145 dB) than the experimental one. We conclude this part by noticing that on this academic set-up, the limitation occurs at a very high acoustic levels 150 dB, actually above the pain threshold of the human ear. In fact, we design the setup to study the physics of the phenomenon, without a particular application in mind. However, in the view of applications, the level of limitation will have to be adapted to the situation.

7. The self-tuning property

After presenting the main physical phenomena observed with the coupling of an acoustic medium to a nonlinear oscillator, we present in this section a very important property of this nonlinear absorber: its ability to adapt and tune itself to the resonance frequency of different linear systems. To demonstrate experimentally this property, we recorded the free oscillations of the system with a given membrane configuration and three different lengths of the tube. Changing this length, we change the linear primary system and its resonance frequency. The membrane configuration taken here is $h=0.39$, $R=30$ mm, $f_1=52$ Hz and the three lengths of the tube are 2.26, 1.8 and 1.55 m. These lengths correspond, respectively, to the resonance frequencies 78, 99 and 112 Hz for the acoustic medium of the set-up. Fig. 29 shows the free oscillations of the system after a sinusoidal forcing at the resonance frequency of the primary system for these three lengths. The amplitudes of the forcing are chosen in order to have the same acoustic level in the tube (around 1000 Pa). We observe that, even if the threshold of the energy pumping and the shape of the curves are different when changing the length, the membrane remains able to capture the resonance of the primary system and to show a targeted energy transfer.

Secondly, in Fig. 30 the simulations of the frequency responses for these three cases are shown. For each length, we present the frequency response of the system with a low amplitude sweep sinus forcing, to have the original resonance peak of the acoustic medium (at 78, 99 and 112 Hz here), and with a higher enough amplitude to observe the clipping of the peak. The important fact is that last observation has always been possible, with the three lengths and of course for any intermediate length. The membrane, as an almost pure nonlinear oscillator, is able to work with any linear primary system having their resonance frequency in a large frequency range, tuning itself on it. This property is an important advantage in comparison to a linear tuned absorber which can only work at a single frequency.

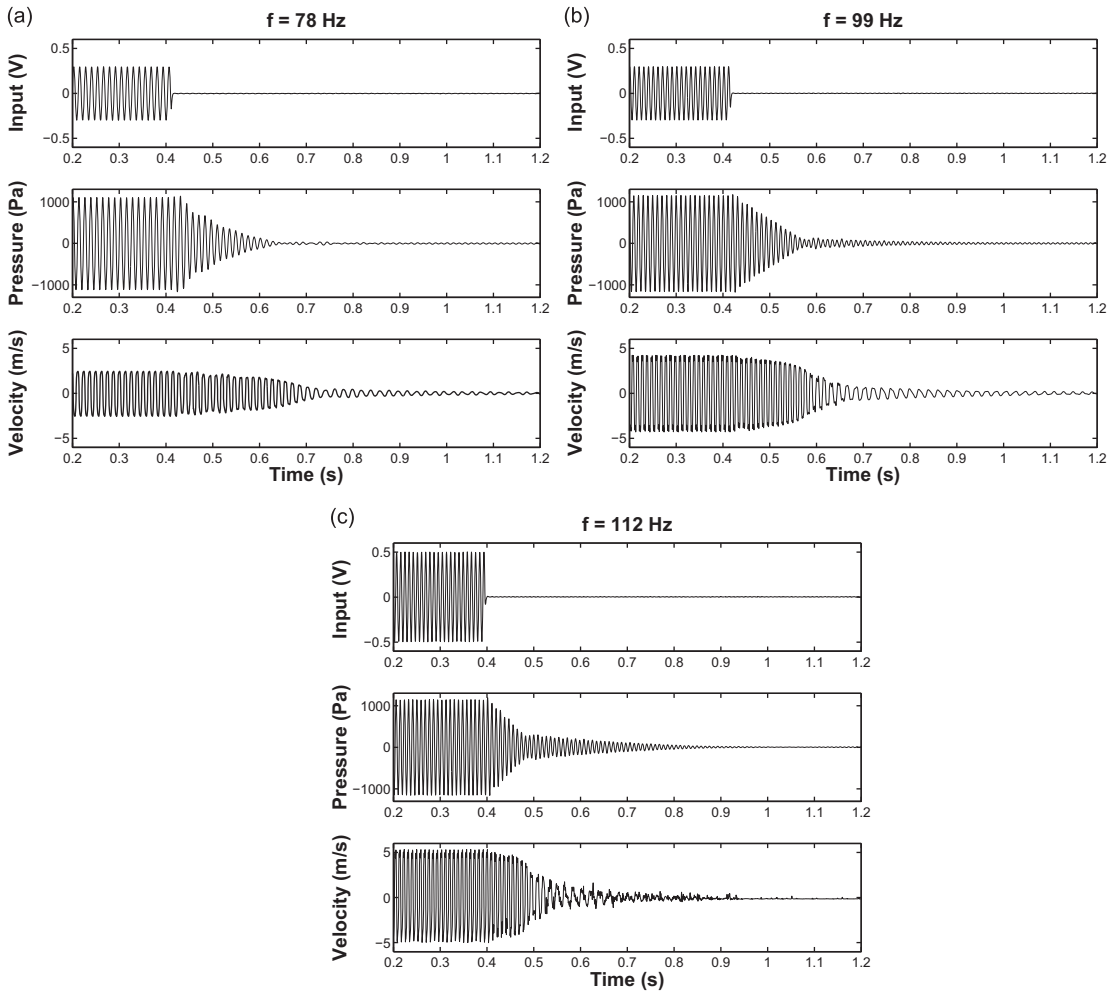

Fig. 29. *Experimental result*. Free oscillations of the system for three different linear primary systems (three different lengths of the tube) with the same membrane configuration. (a) Length of the tube L=2.26 m. (b) Length of the tube L=1.8 m. (c) Length of the tube L=1.55 m.

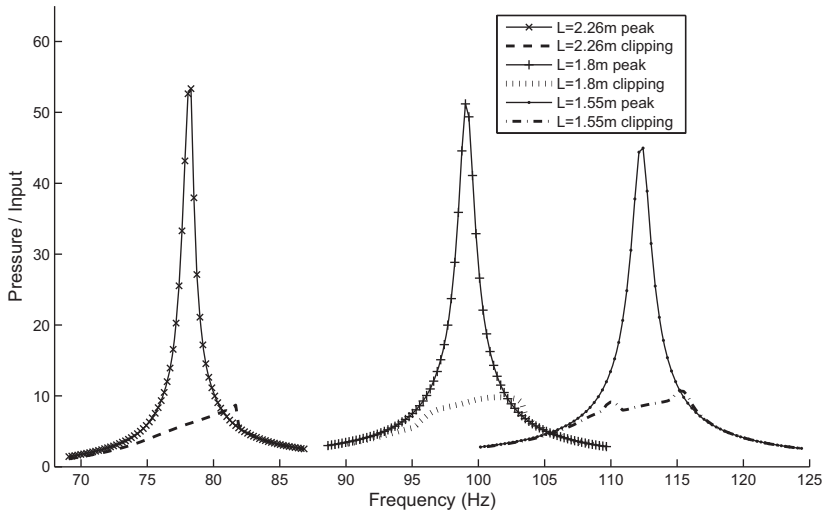

Fig. 30. *Numerical result*. Simulation of the frequency responses for three lengths of the tube.

8. Conclusion

A first observation of targeted energy transfer in acoustics has been achieved in 2006 thanks to a simple set-up and has been reported in a brief paper [33].

In the present paper, a substantially more complete study of targeted energy transfer between an acoustic primary medium and a nonlinear membrane absorber is presented. The set-up used here consisted of a tube with variable length (linear primary system), a coupling box and a visco-elastic membrane (nonlinear absorber) with a holding device allowing to control the membrane radius and pre-stress. Thanks to it, numerous experimental results in agreement with the literature are shown. Irreversible energy transfer was observed in both free and forced regimes as well as frequency responses, using suitable presentations of experimental data such as wavelet transforms and frequency–energy plots. A two dof Rayleigh–Ritz reduction technique with appropriate shape functions also yielded a simple but effective two dof model which accurately matched the main experimental observations. Finally, and this is a main point, we have shown experimentally that a given membrane absorber is able to work with various primary acoustic systems, tuning itself on their different resonance frequencies. Considering that there is no existing efficient dissipative mechanism in acoustics for low frequencies, this work gives very encouraging prospects towards the development a novel kind of low frequency acoustic absorbers.

Acknowledgements

The authors would like to warmly thank S. Bellizzi for helpfull discussions and suggestions as well as G. Kerschen and S. Pernot for their useful time–frequency tools. This research was supported by French National Research Agency in the context of the ADYNO project (ANR-07-BLAN-0193).

References

[1] H. Frahm, A device for damped vibrations of bodies, U.S. Patent, 989959, 1909.
[2] J. Ormondroyd, J. Den Hartog, Theory of the dynamic vibration absorber, *Transactions of the American Society of Mechanical Engineers* 50 (1928) 9–22.
[3] J. Den Hartog, *Mechanical Vibrations*, McGraw-Hill, New York, 1934, pp. 87–106.
[4] A. Thompson, Auxilary mass throw in a tuned and damped vibration absorber, *Journal of Sound and Vibration* 70 (1980) 481–486.
[5] S. Randall, D. Halsted, D. Taylor, Optimum vibration absorbers for linear damped systems, *Journal of Mechanical Design* 103 (1981) 908–913.
[6] A. Thompson, Optimum tuning and damping of a dynamic vibration absorber applied to a force excited and damped primary system, *Journal of Sound and Vibration* 77 (1981) 403–415.
[7] O. Gendelman, L. Manevitch, A. Vakakis, R. M'Closkey, Energy pumping in nonlinear mechanical oscillators: part I—dynamics of the underlying hamiltonian systems, *Journal of Applied Mechanics* 68 (2001) 34–41.
[8] A. Vakakis, O. Gendelman, Energy pumping in nonlinear mechanical oscillators: part II—resonance capture, *Journal of Applied Mechanics* 68 (2001) 42–48.
[9] A. Vakakis, Inducing passive nonlinear energy sinks in vibrating systems, *Journal of Vibration and Acoustics* 123 (2001) 332.
[10] A. Vakakis, L. Manevitch, O. Gendelman, L. Bergman, Dynamics of linear discrete systems connected to local, essentially non-linear attachments, *Journal of Sound and Vibration* 264 (2003) 559–577.
[11] A. Vakakis, R. Rand, Non-linear dynamics of a system of coupled oscillators with essential stiffness non-linearities, *International Journal of Non-Linear Mechanics* 39 (2004) 1079–1091.
[12] D. McFarland, L. Bergman, A. Vakakis, Experimental study of non-linear energy pumping occurring at a single fast frequency, *International Journal of Non-Linear Mechanics* 40 (2005) 891–899.
[13] A. Vakakis, L. Manevitch, A. Musienko, G. Kerschen, L. Bergman, Transient dynamics of a dispersive elastic wave guide weakly coupled to an essentially nonlinear end attachment, *Wave Motion* 41 (2005) 109–132.
[14] F. Georgiades, A. Vakakis, G. Kerschen, Broadband passive targeted energy pumping from a linear dispersive rod to a lightweight essentially non-linear end attachment, *International Journal of Non-Linear Mechanics* 42 (2007) 773–788.
[15] P. Panagopoulos, A. Vakakis, S. Tsakirtzis, Multi-scaled analysis of the damped dynamics of an elastic rod with an essentially nonlinear end attachment, *International Journal of Solids and Structures* 41 (2004) 6505–6528.
[16] P. Panagopoulos, F. Georgiades, S. Tsakirtzis, A. Vakakis, L. Bergman, Multi-scaled analysis of the damped dynamics of an elastic rod with an essentially nonlinear end attachment, *International Journal of Solids and Structures* 44 (2007) 6256–6278.
[17] F. Georgiades, A. Vakakis, Dynamics of a linear beam with an attached local nonlinear energy sink, *Communications in Nonlinear Science and Numerical Simulation* 12 (2007) 643–651.
[18] F. Georgiades, A. Vakakis, Passive targeted energy transfers and strong modal interactions in the dynamics of a thin plate with strongly nonlinear attachments, *International Journal of Solids and Structures* 42 (11–12) (2009) 773–788.
[19] G. Kerschen, J. Kowtko, D. McFarland, L. Bergman, A. Vakakis, Theoretical and experimental study of multimodal targeted energy transfer in a system of coupled oscillators, *Nonlinear Dynamics* 47 (2007) 285–309.
[20] L. Manevitch, O. Gendelman, A. Musienko, A. Vakakis, L. Bergman, Dynamic interaction of a semi-infinite linear chain of coupled oscillators with a strongly nonlinear end attachment, *Physica D* 178 (2003) 1–18.
[21] Y. Lee, A. Vakakis, L. Bergman, D. McFarland, G. Kerschen, Suppression of aeroelastic instabilities by means of targeted energy transfers: part I, theory, *AIAA Journal* 45 (3) (2007) 693–711.
[22] Y. Lee, G. Kerschen, D. McFarland, W. Hill, C. Nichkawde, T. Strganac, L. Bergman, A. Vakakis, Suppression of aeroelastic instability by means of broadband TET: part II, experiments, *AIAA Journal* 45 (2007) 2391–2400.
[23] E. Gourdon, N. Alexander, C. Taylor, C. Lamarque, S. Pernot, Nonlinear energy pumping under transient forcing with strongly nonlinear coupling: theoretical and experimental results, *Journal of Sound and Vibration* 300 (2007) 522–551.
[24] F. Nucera, F. Lo Iaconoa, D. McFarland, L. Bergman, A. Vakakis, Application of broadband nonlinear targeted energy transfers for seismic mitigation of a shear frame: experimental results, *Journal of Sound and Vibration* 313 (2008) 57–76.
[25] R. Viguié, G. Kerschen, J.-C. Golinval, D. McFarland, L. Bergman, A. Vakakis, N. van de Wouw, Using passive nonlinear targeted energy transfer to stabilize drill-string systems, *Mechanical Systems and Signal Processing* 23 (1) (2009) 148–169.

[26] F. Nucera, A. Vakakis, D. McFarland, L. Bergman, G. Kerschen, Targeted energy transfers in vibro-impact oscillators for seismic mitigation, *Nonlinear Dynamics* 50 (2007) 651–677.
[27] O. Gendelman, Targeted energy transfer in systems with non-polynomial nonlinearity, *Journal of Sound and Vibration* 315 (2008) 732–745.
[28] Y. Lee, A. Vakakis, L. Bergman, D. McFarland, G. Kerschen, Enhancing robustness of aeroelastic instability suppression using MDOF energy sinks, *AIAA Journal* 46 (6) (2008) 1371–1394.
[29] S. Tsakirtzis, G. Kerschen, P. Panagopoulos, A. Vakakis, Multi-frequency nonlinear energy transfer from linear oscillators to mdof essentially nonlinear attachments, *Journal of Sound and Vibration* 285 (2005) 483–490.
[30] S. Tsakirtzis, A. Vakakis, P. Panagopoulos, Broadband energy exchanges between a dissipative elastic rod and a multi-degree-of-freedom dissipative essentially non-linear attachment, *International Journal of Non-Linear Mechanics* 42 (2007) 36–57.
[31] S. Tsakirtzis, P. Panagopoulos, G. Kerschen, O. Gendelman, A. Vakakis, L. Bergman, Complex dynamics and targeted energy transfer in linear oscillators coupled to multi-degree-of-freedom essentially nonlinear attachments, *Nonlinear Dynamics* 48 (2007) 285–318.
[32] A. Vakakis, O. Gendelman, L. Bergman, D. McFarland, G. Kerschen, Y. Lee, *Nonlinear targeted energy transfer in mechanical and structural systems*, *Solid Mechanics and its Applications*, Vol. 156, Springer, Berlin, 2008.
[33] B. Cochelin, P. Herzog, P.-O. Mattei, Experimental evidence of energy pumping in acoustics, *C. R. Mecanique* 334 (11) (2006) 639–644.
[34] G. Kerschen, A. Vakakis, Y. Lee, D. McFarland, J. Kowtko, L. Bergman, Energy transfers in a system of two coupled oscillators with essential nonlinearity: 1:1 resonance manifold and transient bridging orbits, *Nonlinear Dynamics* 42 (2005) 283–303.
[35] Y. Lee, G. Kerschen, A. Vakakis, P. Panagopoulos, L. Bergman, D. McFarland, Complicated dynamics of a linear oscillator with a light, essentially nonlinear attachment, *Physica D* 204 (2005) 41–69.
[36] O. Gendelman, D. Gorlov, L. Manevitch, A. Musienko, Dynamics of coupled linear and essentially nonlinear oscillators with substantially different masses, *Journal of Sound and Vibration* 286 (2005) 1–19.
[37] O. Gendelman, C. Lamarque, Dynamics of linear oscillator coupled to strongly nonlinear attachment with multiple states of equilibrium, *Chaos, Solitons and Fractals* 24 (2005) 501–509.
[38] G. Kerschen, Y. Lee, A. Vakakis, D. McFarland, L. Bergman, Irreversible passive energy transfer in coupled oscillators with essential nonlinearity, *Journal of Applied Mathematics* 66 (2006) 648–679.
[39] L. Manevitch, E. Gourdon, C. Lamarque, Parameters optimization for energy pumping in strongly nonhomogeneous 2 dof system, *Chaos, Solitons and Fractals* 31 (2007) 900–911.
[40] G. Kerschen, O. Gendelman, A. Vakakis, L. Bergman, D. McFarland, Impulsive periodic and quasi-periodic orbits of coupled oscillators with essential stiffness nonlinearity, *Communications in Nonlinear Science and Numerical Simulation* 13 (2008) 959–978.
[41] Y. Starosvetsky, O. Gendelman, Dynamics of a strongly nonlinear vibration absorber coupled to a harmonically excited two-degree-of-freedom system, *Journal of Sound and Vibration* 312 (2008) 234–256.
[42] Y. Starosvetsky, O. Gendelman, Response regimes of linear oscillator coupled to nonlinear energy sink with harmonic forcing and frequency detuning, *Journal of Sound and Vibration* 315 (2008) 746–765.
[43] D. Quinn, O. Gendelman, G. Kerschen, T. Sapsis, L. Bergman, A. Vakakis, Efficiency of targeted energy transfers in coupled nonlinear oscillators associated with 1:1 resonance captures: part I, *Journal of Sound and Vibration* 311 (2008) 1228–1248.
[44] A. Leissa, *Vibration of Plates*, Acoustical Society of America, 1993.
[45] G. Kerschen, M. Peeters, J. Golinval, A. Vakakis, Nonlinear normal modes, part I: a useful framework for the structural dynamicist, *Mechanical Systems and Signal Processing* 23 (1) (2009) 170–194.
[46] O. Gendelman, E. Gourdon, C. Lamarque, Quasiperiodic energy pumping in coupled oscillators under periodic forcing, *Journal of Sound and Vibration* 294 (2006) 651–662.
[47] Y. Starosvetsky, O. Gendelman, Strongly modulated response in forced 2DOF oscillatory system with essential mass and potential asymmetry, *Physica D* 237 (2008) 1719–1733.
[48] P. Mattei, High-order perturbation expansion for the spectral analysis of fluid-loaded vibrating structure, *Acta Acustica* 93 (2006) 305–313.
[49] N. Roozen, M. Bockholts, P. van Eck, A. Hirshberg, Vortex sound in bass-reflex ports of loudspeaker. Part I. observation of response to harmonic excitation and remedial measure, *Journal of the Acoustical Society of America* 104 (4) (1998) 1914–1918.
[50] J.-C. Valiere, F. Kerherve, P. Herzog, Non-linéarités générées au niveau des évents d'enceintes (nonlinearities induced in loudspeaker ports), 6e Congrès Français d'Acoustique (French Conference of Acoustics), paper 76, 2002, pp. 1–5.